Int J Earth Sci (Geol Rundsch) (2006) 95: 370–394
DOI 10.1007/s00531-005-0046-6

ORIGINAL PAPER

Abdurrahman Dokuz · Erkan Tanyolu · Salim Genç

A mantle- and a lower crust-derived bimodal suite in the Yusufeli (Artvin) area, NE Turkey: trace element and REE evidence for subduction-related rift origin of Early Jurassic Demirkent intrusive complex

Received: 27 April 2004 / Accepted: 4 September 2005 / Published online: 2 December 2005

Abstract The Yusufeli area, in the Eastern Black Sea Region of Turkey, contains a crystalline complex that intruded into the Carboniferous metamorphic basement and is composed of two intrusive bodies: a gabbro-diorite and a tonalite-trondhjemite. The mafic body (45–57 wt% SiO_2) displays a broad lithological spectrum ranging from plagioclase-cumulate to quartz diorite. Primitive varieties of the body have Mg-number, MgO and Cr contents that are close to those expected for partial melts from mantle peridotite. Data are consistent with the magma generation in an underlying mantle wedge that was depleted in Zr, Nb and Ti, and enriched in large ion lithophile elements (K, Rb, Ba, Th). However, high Al_2O_3, CaO and generally low Ni (< 65 ppm) contents are not in agreement with the unfractionated mantle-derived primitive magmas and require some Al_2O_3- and CaO-poor mafic phases, in particular, olivine and orthopyroxene. Absence of orthopyroxene in crystallization sequence, uralitization, and a common appearance of clinopyroxene surrounded by hornblende imply an anhydrous phase fractionated from highly hydrous (5–6%) parent. Geochemical modelling suggests derivation by 15–20% melting of a depleted-lherzolitic mantle. The tonalite-trondhjemite body (58–76 wt% SiO_2) ranges in composition from quartz diorite to granodiorite with a low-K calc-alkaline trend. Although LILE- and LREE- enriched characteristics of the primitive samples imply a metasomatic sub-arc mantle for their source region, low MgO, Ni and Cr concentrations rule out direct derivation from the mantle wedge. Also, lack of negative Eu anomalies suggests an unfractionated magma and precludes a differentiation from the diorites of mafic body, which show negative Eu anomalies. Their Na enrichments relative to Ca and K are similar to those of Archean tonalites, trondhjemites and granodiorites and Cenozoic adakites. However, they exhibit important geochemical differences from them, including low-Al (< 15 wt%) contents, unfractionated HREE patterns and evolution towards the higher Y concentrations and lower Sr/Y ratios within the body. All these features are obtained in experimentally produced melts from mafic rocks at low pressures (≤ 5 kbar) and also widespread in the rocks of arc where old (Upper Cretaceous or older) oceanic crust is being subducted. Major and REE modelling supports formation of the quartz dioritic parent to the felsic intrusive rocks by 70% partial melting of a primitive gabbroic sample (G694). Therefore, once taking into account the extensional conditions prevailing in the Pontian arc crust in Early Jurassic time, former basic products (gabbros) seem to be the most appropriate source for the tonalite-trondhjemite body. Magmatic emplacement of stratigraphically similar lithologies in the Pulur Massif, just southwest of the Yusufeli, was dated to be 184 Ma by the $^{40}Ar/^{39}Ar$ method on amphibole, and is compatible with the initiation of Early Jurassic rifting in the region.

Keywords Low-K bimodal suite · Trace elements · Crystallization conditions · Subduction · Rifting · Emplacement · Demirkent intrusive complex · Yusufeli-Artvin · Eastern Pontides · Turkey

A. Dokuz (✉) · S. Genç
Department of Geology, Karadeniz Technical University,
29000 Gümüşhane, Turkey
E-mail: dokuz@ktu.edu.tr
Tel.: +90-456-2337425
Fax: +90-456-2337427

E. Tanyolu
Department of Geology, Fırat University,
23119 Elazığ, Turkey
E-mail: etanyolu@firat.edu.tr

Introduction

Palaeozoic rocks in the Eastern Pontian arc occupy nearly 10% of the whole area, mainly on the southern flank of the arc, and are conventionally known as a Hercynian or a Palaeozoic basement. The regionally

metamorphosed gneisses and schists are the dominant rock types in the basement. Minor constituents include mafic/ultramafic to felsic rocks that intruded into pre-existing metamorphic suites. Comparison of the geology, geochemistry and petrogenesis of these intrusive rocks show that they are separable into two groups in terms of their source areas, age of formation and stress conditions affecting the crust during their emplacement. The first group is the medium- to high-K granitoids, such as the Gümüşhane granitoid pluton (Yılmaz 1972; Çoğulu 1975) and the Köse granitoid pluton (Bergougnan 1987), which are relatively abundant and larger than the mafic/ultramafic intrusions and formed during the Hercynian orogeny. The other group is the low-K bimodal suites found in Upper Palaeozoic metamorphics, such as the Pulur Massif, south of Bayburt (Topuz 2002), and the Yusufeli-Artvin metamorphics (Dokuz 2000), as cross-cutting relatively small intrusives, which formed during the Early Jurassic arc rifting.

Although all the intrusive complexes cutting the metamorphic basement generally have been evaluated as the subduction products formed in the overlying volcanic arc during the consumption of Paleo-Tethyan ocean floor, there are also considerable disagreements concerning the petrogenetic and geodynamic evolution of these rocks. The Demirkent intrusive complex from the Yusufeli area has played an important role in model studies concerning the Late Palaeozoic to Early Jurassic geological history of the Eastern Pontides. These crystalline rocks and stratigraphically similar lithologies in other domains (e.g. Kelkit and Sinop-Daday areas) were included in an oceanic assemblage and have been interpreted as being remnants of Permian-Triassic Paleo-Tethys (Şengör et al. 1980; Şengör and Yılmaz 1981; Yılmaz et al. 1997). Moreover, Adamia et al. (1995) named these crystalline rocks as Ahalt massif and suggested that clinopyroxenes of gabbros and diabases have been strongly uralitized and that their bulk composition corresponds to oceanic basaltic and plutonic rocks with a very distinct tholeiitic trend. In addition, tonalites and trondhjemites of the complex have been interpreted as plagiogranites due to their low K_2O contents. On the other hand, Konak and Hakyemez (1996) have suggested that there is no similarity to sheeted-dike complexes of the ophiolite suite, although they named the same rocks as Demirkent Dike Complex. They also proposed that these rocks are of tholeiitic composition, have an island-arc character, and were developed in a paleo-subduction zone. In addition, mafic and ultramafic parts of these crystalline complexes have been interpreted as Alaskan-type cumulative ultramafic rocks including biotite and hornblende, forming the root of the Eastern Pontide magmatic arc (Bektaş and Güven 1995). It is therefore clear that the determination of the major and trace element characteristics of the crystalline rocks found in the basement is crucial to find out in which tectonic environments these rocks formed and to understand of the Late Palaeozoic to Early Mesozoic tectonic history of the Eastern Pontides in general. When considered together with the other pre-Jurassic crystalline rocks, further study of these crystalline rocks is critical to test radically different models of Paleo-Tethyan evolution and to understand petrogenetic processes accompanying the formation of these two different generations.

In this paper, we report for the first time the petrologic, geochemical and field characteristics of the Early Jurassic Demirkent intrusive complex. The well-preserved magmatic fabrics and mineralogy of the mafic and felsic rocks with their mineral analyses permit postulation of crystallization sequences and estimates of emplacement depths.

Summary of the basement geology of the Eastern Pontides

The Eastern Pontides form a 500 km long and 100 km wide mountain chain along the southeastern coast of the Black Sea (Fig. 1). The Eastern Pontides are well known as one of the best-preserved examples of a paleo-island arc of the Late Palaeozoic age (Akin 1978; Şengör and Yılmaz 1981; Akıncı 1984; Okay and Şahintürk 1997; Yılmaz et al. 1997). The pre-Jurassic basement is exposed in only a number of small isolated areas and has a limited range of rock types in the Eastern Pontides. Tokat Massif, situated in the westernmost part of the Eastern Pontides, has the largest exposure. The other basement outcrops are, from the west to the east, Ağvanis Massif, Gümüşhane-Bayburt metamorphics, Pulur Massif and Yusufeli-Artvin metamorphics. All the massifs display broadly similar geological features and may be regarded as the basement to the post-Triassic rocks. Rock types of these basement units can be grouped mainly into two: a medium to high-grade metamorphic complexes of Carboniferous age, and a cutting pre/Early Jurassic granitoid complexe.

The metamorphic complexes vary mineralogically and texturally from quartzo-feldspatic gneiss (Yılmaz 1972; Tanyolu 1988; Okay 1996; Dokuz 2000; Topuz et al. 2004) to metabasite (Alp 1972; Okay 1984; Aktimur et al. 1992) in Eastern Pontides. Sm–Nd garnet-whole rock age of 330 Ma for the mesocratic gneisses and $^{40}Ar/^{39}Ar$ muscovite age of 314.9 ± 2.4 Ma (and Rb–Sr muscovite age of ~315 Ma) yielded for the pegmatites have been suggested as the time of peak and cooling metamorphic conditions, respectively, of the Massif (Topuz et al. 2004).

Pre/Early Jurassic granitoid complexes are represented volumetrically in high proportion by Early Carboniferous to Permian granitoid plutons lying on the southern flank of the Eastern Pontides. Although they include a variety of granitic rocks with a medium-K calc-alkaline trend, hornblende-biotite granodiorite and adamellite make up the main bodies of the plutons (Yılmaz 1972; Bergougnan 1987). The Gümüşhane granitoid pluton approximately dated to be 298–338 Ma by the whole-rock Pb isotope method (Çoğulu 1975), whereas

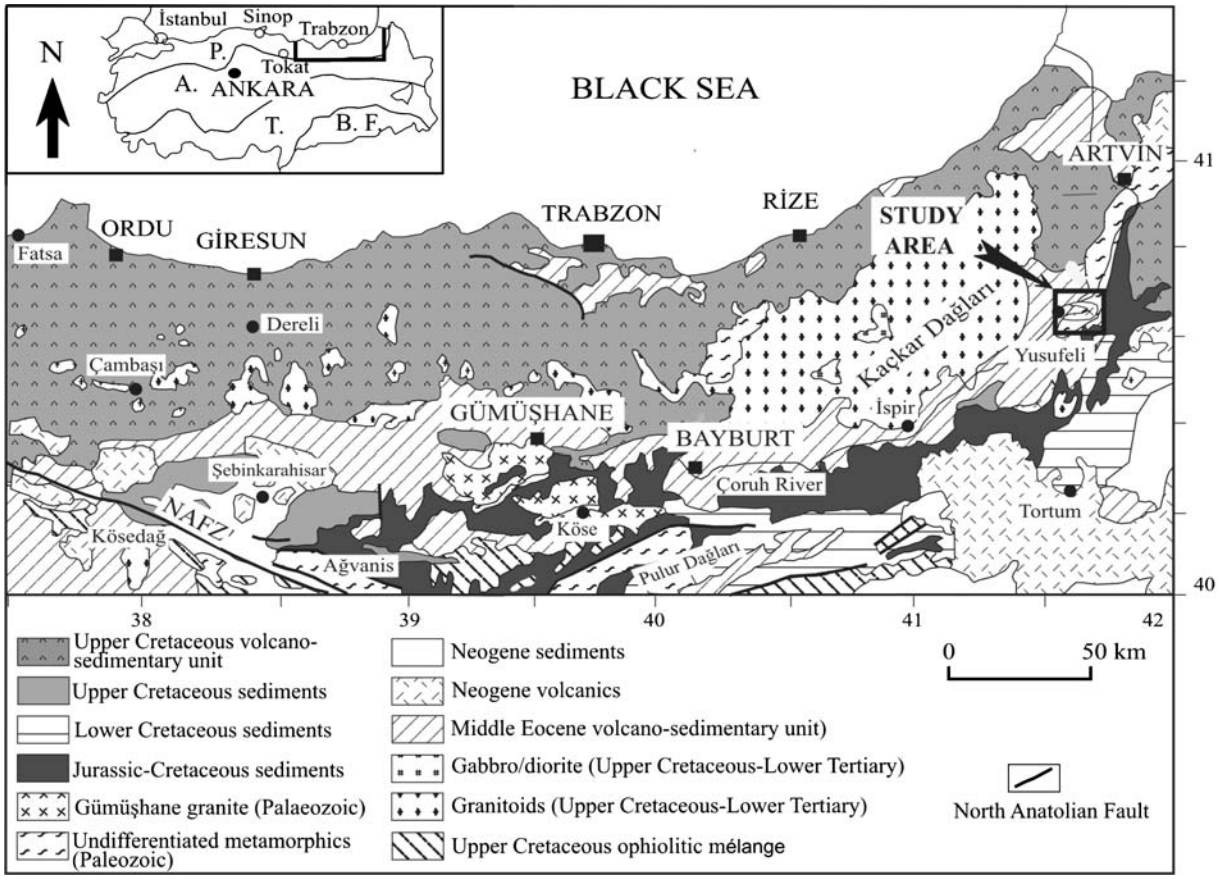

Fig. 1 Simplified geological map of the Eastern Black Sea region (after the geological map of Turkey with a scale of 1/500,000, MTA 1961) and the location of the area mapped in detail. *Inset* shows the tectonic units of Turkey with the location of Eastern Pontides in it. *P* pontides, *A* anatolides, *T* taurides and *BF* border folds (from Ketin 1966)

the Köse granitoid pluton has yielded a well-defined earliest Carboniferous (360 ± 2 Ma) Rb/Sr isochron age (Bergougnan 1987). Another type of granitic intrusion associated with the metamorphic basement of the Eastern Pontides is a bimodal intrusive suite, but such intrusive bodies are much smaller and low-K gabbro-trondhjemitic in character (Dokuz 2000), and seem to be younger than the medium to high-K Carboniferous granitoids. A mafic to ultramafic complex intruded into the metamorphic rocks of the Pulur Massif, southwest of Bayburt, has yielded a well-defined plateau age of 184.2 ± 4.4 Ma (Early Jurassic) by $^{40}Ar/^{39}Ar$ method on amphibole (Topuz 2002).

Geology of the Yusufeli area basement rocks

The Yusufeli area is located about 75 km south of Artvin, at the eastern end of the Black Sea. There are numerous studies of the investigated area along the Sarp-Artvin-Erzurum traverse, carried out by the General Directorate of Mineral Research and Exploration [Maden Tetkik ve Arama Enstitüsü (MTA)]. These investigations were aimed principally at the mapping of the areas. The area has been further mapped (Fig. 2) and investigated in detail more recently by Konak and Hakyemez (1996) and Dokuz (2000).

The Yusufeli area is one of the very few areas comprising both the Hercynian crystalline basement together with the Early Jurassic bimodal intrusives and the Jurassic to Middle Eocene sedimentary cover. Lithologically, the basement seems to be a northeasterly extension of the Pulur Massif, southwest of Bayburt, elongated in a NE–SW direction and including the metamorphic rocks of Yusufeli area. Dokuz (2000) first studied the geology of the region in detail (Fig. 2). Rock types of the basement are quite similar to those of the basement geology of the Eastern Pontides. The oldest unit in the crystalline basement, named the Karadağ metamorphics, is composed of lithologically varied schists, gneisses and metabasites. All these rocks have generally medium to strong schistosity and in some places gneisses show ptygmatic structure and migmatitic texture. Some parts of the metamorphics have been extensively mylonitized. There is no age determination for the metamorphics. As for metamorphism age, the Middle Carboniferous age is assigned to the metamorphics on the basis of analogy to the high-grade metamorphics of the Pulur Massif (Topuz et al. 2004). These crystalline metamorphics were cut first by an Early

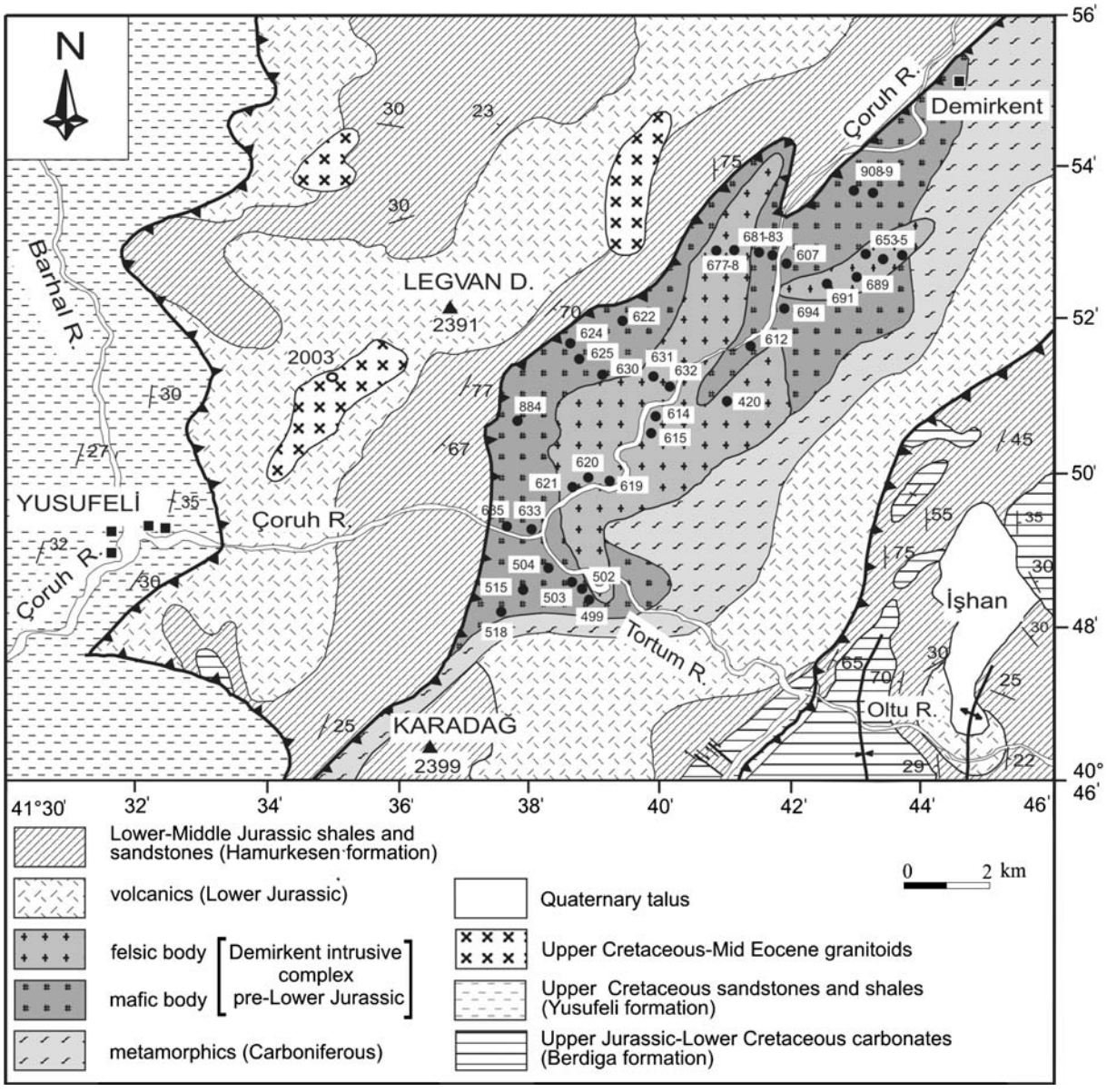

Fig. 2 Detailed geological map of the Yusufeli (Artvin) area including locations of the analysed samples (after Dokuz 2000)

Jurassic mafic intrusive. This mafic intrusive body has an area of 30 km^2 and an elliptical shape with NE–SW trending long axis and lithologically ranges from plagioclase-cumulate to quartz diorite. All these lithologies show gradational transition to each other with textural transformations.Textural transitions and transformations are best shown between the gabbros and gabbro-pegmatites in the field in decimetre scale. The metamorphics and the mafic intrusion were later cut by two felsic intrusives, which are made up mainly of tonalite, trondhjemite and subordinately quartz diorite and granodiorite. They cover areas of about 2 and 20 km^2, respectively, and the latter was emplaced nearly into the central part of the mafic intrusion. As a result of this, the mafic intrusion took a concentric appearance surrounding the felsic intrusion. The felsic intrusion has also a linear shape elongating in the same direction as the mafic intrusion and an extremely straight linear and a vertical contact with the mafic intrusion along the northeastern boundary. In places, dikes of the felsic intrusion alternate with wall rocks of the mafic intrusion; but this pattern does not occur throughout the entire intrusive complex as implied in prior studies (Konak and Hakyemez 1996). This structure, probably indicating the importance of structural elements during the emplacement of the felsic intrusion melt, was intensely developed only along the northern and the southern margins of the felsic intrusion. It differs from sheeted-dike complexes in the spacing of the dikes within a country rock. Strikes of these dikes are largely parallel to the general direction of long axis of the intrusions. In many places, fragments of the wall rocks can be

observed as isolated bodies or mega inclusions in the dike system. In some places, especially at the junction of the Çoruh and Tortum Rivers (Fig. 3), the wall rocks of the mafic intrusion are cut irregularly by veins branching from the felsic dikes in various directions. Their age of emplacement into the metamorphic basement can be evaluated as Early Jurassic because of their elaborate similarity to those dated as being 184 ± 4.4 Ma in the Pulur Massif (Topuz 2002). All the basement rocks were thrusted over the unconformably overlying Mesozoic cover units along their northwestern boundary during the Cenozoic compressive events.

Analytical procedure

Over 100 samples from the Demirkent intrusive complex outcrops were collected. Of these, 36 samples have been analysed. Bulk-rock chemical compositions of the samples were determined by inductively coupled plasma-mass spectrometry (ICP-MS) at the commercial Acme Analytical Laboratories Ltd. in Vancouver, Canada. In the ICP-MS analyses, a 0.2 g aliquot was weighed into a graphite crucible and mixed with 1.5 g of $LiBO_2$ flux. Crucibles are placed in an oven and heated to 1,050°C for 15 min. The molten sample is dissolved in 5% HNO_3 (ACS grade nitric acid diluted in demineralized water). Calibration standards and reagent blanks are added to the sample sequence. Sample solutions are aspirated into an ICP emission spectrograph (Jarrel Ash Atom Comb 975) for major oxides and certain trace elements (Ba, Nb, Ni, Sr, Sc, Y and Zr), while the sample solutions are aspirated into an ICP mass spectrometer (Perkins-Elmer Elan 6000) for determination of the trace elements including rare earth elements. Accuracy for major elements is 2% and for trace elements 10%.

Mineral analyses were carried out with a five spectrometer CAMECA-SX51 electron microprobe equipped with five wavelength-dispersive spectrometers and an additional Si–Li detector (Oxford Instruments) at the Mineralogical Institute of Heidelberg University. Natural and synthetic oxide and silicate standards were used for calibration before each measurement session. Standard operating conditions were a 15 kV accelerating voltage, 20 nA beam current and 10 s counting times for all the elements except for those in feldspars. A beam size of 1 μm was used in analyses except for plagioclases. Feldspar analyses were conducted on a beam size of ~10 μm to minimize the alkali loss due to volatilization and to integrate microperthitic lamella. Raw data were corrected for matrix effects with the help of the PAP algorithm (Pouchou and Pichoir 1985) implemented by CAMECA. Detection limits are generally in the order of 0.1 wt% of the element under consideration.

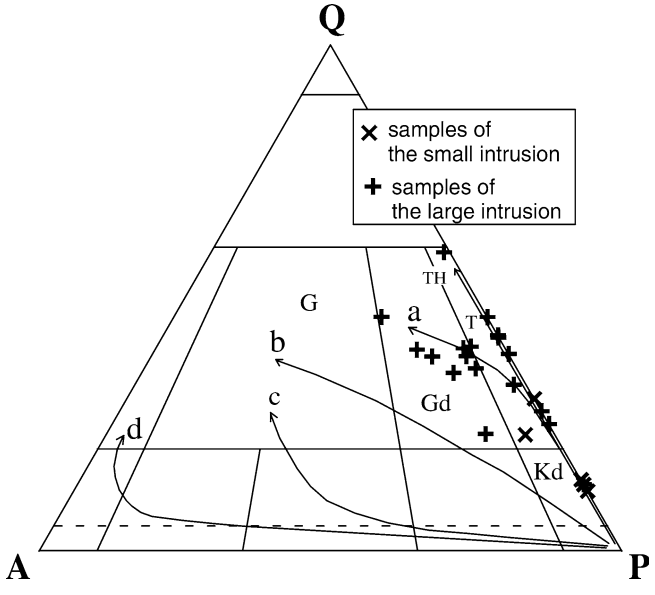

Fig. 3 Modal Q–A–P diagram showing the location of representative points for the felsic rocks of the Early Jurassic Demirkent intrusive complex in the field of quartz diorite, tonalite and granodiorite according to the Streckeisen (1976) classification. *Kd* quartz diorites, *T* tonalites (and trondhjemites), *Gd* granodiorites, and *G* granites. *Arrows* show typical differentiation trends (after Lameyre and Bowden 1982) for various magmatic series: tholeiitic (TH), K_2O-poor calc-alkaline (**a**), intermediate K_2O content calc-alkaline (**b**), K_2O-rich calc-alkaline (**c**), and alkali (**d**). The representative points for the felsic rocks of Early Jurassic Demirkent intrusive complex closely follow a K_2O-poor calc-alkaline trend

Results

Petrography and mineral chemistry

The petrographic names of rocks of the Demirkent intrusive complex presented below are based on modal mineral composition obtained by point counting. The mafic intrusion grades from gabbro to quartz diorite but gabbro (more common) and diorite constitute the main body. The rocks of the felsic intrusion vary from quartz diorite to granodiorite (tonalite the most common) in the classification of Streckeisen (1976) (Fig. 3) with a K_2O-poor calc-alkaline trend (Lameyre and Bowden 1982). As the quartz diorites dominate the small intrusion, and more than half of the modally tonalitic samples of the large intrusion have K-feldspar and colour indices less than 10%, the general characteristic of the intrusion is trondhjemitic. Representative chemical compositions of clinopyroxene (cpx), hornblende (hb) and plagioclase (pl) are given in Table 1.

The mafic intrusion

The mafic inrusive rocks are generally composed of pl, cpx, hb and magnetite with subordinate apatite, k-feldspar (k-fs), quartz (q), epidote ± rutile ± ilmenite. Of these minerals, only pl occurs as cumulus ($An_{65–76}$), while cpx and hb form the intercumulus phase in plagioclase cumulates. Pl crystals, with some needle-shaped laths ($An_{71–81}$) within cpx, are unzoned or weakly zoned

Table 1 Representative electron microprobe analyses (wt%) of clinopyroxene, amphibole and plagioclase, Demirkent intrusive complex

Phase	Plagioclase cumulate				Gabbro			Diorite				Plagioclase cumulate				
Sample	Cpx G681	Cpx G681	Cpx G681	Cpx G681	Cpx G518	Cpx G518	Cpx G518	Cpx G635	Cpx G635	Cpx G635		Hb G681	Hb G681	Hb G681	Hb G681	Hb G518
SiO_2	50.59	51.46	50.87	52.36	51.63	51.76	50.87	51.45	51.64	51.71	SiO_2	50.59	51.46	52.62	51.13	50.76
TiO_2	0.87	0.29	0.59	0.15	0.37	0.55	0.89	0.00	0.00	0.00	TiO_2	0.87	0.29	0.43	0.28	0.93
Al_2O_3	3.96	2.01	4.43	2.21	1.02	2.12	2.79	0.00	0.00	0.00	Al_2O_3	3.96	2.01	6.33	6.12	6.35
FeOt	7.10	5.75	7.22	6.12	11.09	9.52	10.15	17.27	17.09	16.88	FeOt	7.1	5.75	10.30	9.89	11.56
MgO	12.84	13.27	13.41	14.27	12.18	12.74	12.27	9.20	8.23	7.96	MgO	12.84	13.27	17.72	18.85	17.77
MnO	0.16	0.48	0.19	0.51	0.25	0.51	0.44	0.00	0.00	0.00	MnO	0.16	0.48	0.57	0.66	0.57
CaO	24.06	25.93	22.81	23.84	23.02	22.44	22.20	21.68	22.57	22.94	CaO	24.06	25.93	11.57	13.05	11.60
Na_2O	0.42	0.64	0.35	0.53	0.43	0.35	0.40	0.23	0.22	0.33	Na_2O	0.42	0.64	0.45	0.20	0.45
K_2O	0.00	0.17	0.13	0.00	0.00	0.00	0.00	0.17	0.25	0.18	K_2O	0.00	0.17	0.00	0.00	0.00
$\sum$	100	100	100	99.99	99.99	99.99	100.0	100	100	100	$\sum$	100	100	100	100	100
Wo	50.59	52.63	49.37	48.77	47.15	46.75	46.69	45.18	47.65	48.61	Mg#	0.85	0.88	0.87	0.96	0.74
En	37.62	37.48	38.64	40.62	34.71	36.93	35.90	26.70	24.17	23.46						
Fs	11.77	9.88	11.98	10.59	18.13	16.32	17.39	28.11	28.16	27.92						

Phase	Gabbro			Diorite		quartz diorite						Tonalite-trondhjemite				
Sample	Hb G518	Hb G518	Hb G518	Hb G635	Hb G635	Hb T689 Rim	Hb T689 Core	Hb T689 Rim	Hb T689 Rim	Hb T689 Core	Hb T689 Rim	Hb T615 Rim	Hb T615	Hb T615 Core	Hb T615 Core	Hb T615 Rim
SiO_2	51.52	46.30	47.05	49.85	48.74	49.3	48.96	50.93	48.38	48.55	48.65	48.81	47.89	47.81	47.81	47.31
TiO_2	0.61	1.61	1.26	0.55	0.67	1.00	1.14	1.19	1.19	1.29	1.37	1.16	1.57	1.52	1.52	1.22
Al_2O_3	1.94	7.60	7.55	4.70	3.61	6.51	6.68	5.46	6.92	6.84	6.73	6.24	7.01	6.88	6.88	5.64
FeOt	8.45	21.83	22.33	23.25	25.42	15.14	14.93	14.76	13.48	13.5	13.65	15.50	15.44	15.77	15.77	14.83
MgO	0.16	7.97	0.58	0.46	0.51	13.68	13.74	15.21	14.61	14.87	14.70	13.84	12.80	12.82	12.82	13.01
MnO	12.45	0.64	7.16	8.76	8.14	0.71	0.61	0.50	0.39	0.49	0.42	0.46	0.44	0.53	0.53	0.48
CaO	24.37	12.12	12.31	10.75	11.23	10.15	10.52	11.48	10.65	10.77	10.84	10.51	11.38	10.95	10.95	10.68
Na_2O	0.49	1.46	1.51	1.29	1.55	1.09	1.11	0.06	1.53	1.51	1.44	1.33	1.24	1.31	1.31	1.10
K_2O	0.00	0.47	0.25	0.40	0.45	0.15	0.14	0.42	0.14	0.17	0.16	0.17	0.43	0.32	0.32	0.37
$\sum$	100	100	100	100	100	97.75	97.84	100	97.33	98.00	97.97	98.03	98.21	97.94	97.94	94.65
Mg#	0.81	0.39	0.36	0.38	0.43	0.70	0.701	0.71	0.73	0.74	0.73	0.69	0.63	0.64	0.65	0.66

Phase	Pl cumulate			Gabbro		Diorite			Quartz diorite					Ton-trondhjem		
Sample	Pl G681	Pl G681	Pl G681	Pl G518	Pl G518	Pl G635	Pl G635	Pl G635	Pl T689	Pl T689	Pl T689	Pl T689	Pl T689	Pl T613	Pl T613	Pl T613
SiO_2	50.39	49.15	48.04	50.01	56.94	66.95	60.14	64.28	53.03	56.17	60.05	51.57	52.94	63.23	66.38	58.62
TiO_2	0.00	0.18	0.00	0.12	0.21	0.00	0.00	0.00	0.01	0.01	0.03	0.01	0.01	0.01	0.01	0.03
Al_2O_3	31.01	32.17	32.43	31.21	26.65	24.67	26.35	23.69	31.17	27.39	25.01	30.43	29.48	23.42	20.8	25.69
FeOt	0.30	0.28	0.72	0.36	0.24	0.24	0.22	0.21	0.27	0.23	0.18	0.22	0.41	0.14	0.04	0.19
MgO	0.00	0.00	0.00	0.00	0.00	0.00	0.00	0.00	0.02	0.01	0.02	0.01	0.02	0.00	0.00	0.00
MnO	0.33	0.00	0.00	0.35	0.00	0.10	0.08	0.12	0.03	0.03	0.02	0.01	0.00	0.02	0.03	0.03
CaO	14.75	16.24	16.10	13.88	11.70	2.17	7.21	4.82	12.51	9.75	6.96	13.44	12.4	4.31	1.8	6.99
Na_2O	3.21	1.98	2.61	3.95	4.13	5.62	5.42	6.53	2.86	5.87	7.70	3.70	4.39	8.90	9.91	7.23

Table 1 (Contd.)

Phase	Pl cumulate			Gabbro		Diorite			Quartz diorite				Ton-trondhjem			
Sample	Pl G681	Pl G681	Pl G681	Pl G518	Pl G518	Pl G635	Pl G635	Pl G635	Pl T689	Pl T689	Pl T689	Pl T689	Pl T613	Pl T613	Pl T613	Pl T613
K_2O	0.00	0.00	0.09	0.11	0.13	0.08	0.26	0.35	0.06	0.17	0.28	0.10	0.12	0.34	1.11	0.38
P_2O_5	0.00	0.00	0.00	0.00	0.00	0.17	0.31	0.00	0.00	0.02	0.00	0.02	0.02	0.03	0.02	0.03
$\sum$	99.99	100	99.99	99.99	100	100	99.99	100	99.99	99.66	100.3	99.55	99.79	100.4	100.1	99.2
An	71.75	81.93	76.92	65.60	60.54	17.45	41.61	28.26	70.46	63.88	48.81	79.50	75.09	20.70	8.55	34.05
Ab	28.25	18.07	22.56	33.77	38.66	81.78	56.60	69.28	29.14	34.79	48.85	19.80	24.05	77.35	85.17	63.73
Or	0.000	0.000	0.51	0.62	0.80	0.76	1.78	2.44	0.40	1.33	2.34	0.70	0.86	1.94	6.27	2.20

Mg# = $Mg/(Mg+Fe^{2+})$

in plagioclase cumulates, whereas the amount of zoned pl is greater in non-cumulate gabbro, diorite ($An_{14–46}$) and quartz diorites. Cpx, with a composition of diopside in gabbros and diopside-hedenbergite in diorites, was commonly mantled by hb and is poikilitic, with inclusions of generally needle-shaped pl, in plagioclase cumulates. It was generally altered to hb and chlorite in increasing proportions from rim to core and Fe–Ti oxide along the cleavages of grains. Hb is the main ferromagnesian mineral in all the rocks of the mafic intrusion. Generally, it is present as subhedral primary magmatic minerals and as subsolidus reaction products after cpx in decreasing proportions towards the centre of the crystal. Locally, transformation to fibrous actinolitic hb is also widespread. Primary Fe–Ti oxides occur in small to medium aggregates. Apatite is a relatively common accessory mineral shown as rod-like inclusions. Q and k-fs occur as interstitial aggregates in quartz dioritic samples, which volumetrically constitute the least common lithology.

The felsic intrusion

The rocks of the felsic intrusion are composed essentially of pl, q and variable amounts of k-fs, hb and biotite (bi); apatite and zircon are accessory minerals with some magnetite whereas secondary minerals are represented by chlorite, epidote and sericite. All the pl grains are strongly zoned; the cores of these grains vary from $An_{79–60}$ in quartz diorites (modal nomenclature) and $An_{62–50}$ in trondhjemites. These compositions grade gradually to $An_{25–19}$ and to $An_{20–12}$, respectively, in the rims. Pl exhibits variable degree of alteration. Sericite and, occasionally, epidote occupy the pl in decreasing rates from the centre to rim. K-fs is perthitic orthoclase ($Or_{95–84}$) in composition and occurs as interstitial grains in nearly half of the trondhjemite-tonalite samples. Hb, with a magnesio-hb composition, is the main mafic mineral in quartz diorite to tonalitic samples. Alteration of hb to chlorite and actinolite is uncommon in quartz diorite and tonalite but common in trondhjemite and granodiorite. Bi is the second order mafic component in these rocks. Unaltered bi with an annite Fe/(Fe + Mg) = 47–49, and phlogopite Mg/(Fe + Mg) = 51–53 compositon is scarce and is found only in quartz dioritic to tonalitic samples. They are generally chloritized and oxidized along their cleavages.

P–T conditions of crystallization

The intrusions discussed in this study contain hb and pl, which can be used to constrain the *P–T* conditions of crystallization. The method of Al-in-hb barometry of Anderson and Smith (1995) was utilized to deduce the pressure at which the magma crystallized. The total-Al content of hb is a function of both pressure and temperature. The Anderson and Smith (1995) calibration

has an advantage over the other Al-in-hb barometry calibrations of Hammarstrom and Zen (1986), Hollister et al. (1987), Johnson and Rutherford (1989) and Schmidt (1992), as it considers the effect of temperature.

In spite of the fact that the mafic intrusion has suitable mineral assemblage to obtain quantitative *P–T* estimates, low temperature subsolidus alterations is widespread, in particular along the rims of the minerals. A common example is the late-stage alteration of hb rims to actinolite, which, if undetected, will result in anomalously low pressure estimates. Pressure conditions of hb crystallization is calculated to be 2.0–2.5 kbar for the selected unaltered hb analyses from gabbros (Table 2), with lower estimates from the diorites (Table 2), demonstrating low pressure conditions for the crystallization and implying a shallow depth of emplacement for the mafic intrusion.

The felsic intrusion with the mineral assemblage pl, hb, k-fs, bi and magnetite resembles those calcic plutons of Hammarstrom and Zen (1986), which are suitable for estimating crystallization pressures by using Al-in-hb barometry. Crystallization temperatures were calculated from coexisting hb and pl, using the hb-pl thermometer recommended by Blundy and Holland (1990) for quartz-bearing assemblages. The results are shown in Table 2. Accordingly, the *P–T* conditions of crystallization for the felsic intrusion were estimated to be 700–750°C and 1.5–2.0 kbar. Some rim compositions of the hb yield estimates of 0.3–0.5 kbar, which may indicate an extensional or a transtentional condition in the crust during crystallization and/or may have also been caused by some subsolidus transformation to actinolitic hb.

Geochemistry

The mafic intrusion

The mafic rocks are characterized by an extended range of silica (46–58 wt% SiO_2), alumina (15–23 wt% Al_2O_3), magnesium (3–10 wt% MgO), Cr and Ni (Table 3). K_2O, Na_2O and Sr contents are relatively low through the range of composition. In the variation diagrams of SiO_2 versus K_2O (Fig. 4a) and total alkali versus silica (Fig. 4c), the samples scatter along the low-K and subalkalic sides, respectively (Wilson 1989; Peccerillo and Taylor 1976). They have moderate iron enrichments with their Mg-numbers (MgO/MgO + FeO) ranging from 0.31 to 0.75. On an A-F-M ternary diagram (Fig. 5), the rocks lie in the transition between tholeiitic and calc-alkaline character (Irvine and Baragar 1971). On the $FeO^T/(FeO^T + MgO)$–SiO_2 and Al_2O_3–CaO–MgO diagrams (not shown), all of them grouped in the field of mafic cumulates of Coleman (1977). Harker diagrams show clear trends for the most major and trace elements (Fig. 4). Al_2O_3, CaO, MgO, Fe_2O_3, Sr and Sc all show strong negative correlation with SiO_2, whereas Na_2O, Zr, Y, Nb and Ce show strong, and K_2O and TiO_2 show poorer positive correlations.

Figure 6 indicates that all the rock types of the mafic intrusion have depletion in high field strengh trace elements (HFSE), such as Nb, Ta, Zr, Hf and Ti. They show enrichment in large ion lithophile elements (LILE), but some gabbros have low concentrations of U and Th relative to K and Ba. Sr is compatible in plagioclase (Bindeman et al. 1998) and consequently the positive Sr anomaly is in first approximation a function of the amount of plagioclase. Diorites are characterized by negative Sr anomalies in agreement with negative Eu anomalies, indicating possible plagioclase fractionation.

Chondrite-normalized REE diagram of the gabbroic and dioritic rocks (Fig. 7a) shows flat patterns, with values of La_n/Lu_n from 1.48 to 5.37. Total REE abundances increase from gabbros (3× chondrite) to diorites (30× chondrite) and correlate positively with decreasing MgO. Gabbros have higher alumina (18–23 wt% Al_2O_3) values and show positive Eu anomalies. This confirms the presence of some cumulus plagioclase as observed in thin sections. The magnitude of negative Eu anomaly gradually increases whereas Al_2O_3 content decreases towards the diorites and quartz diorites as the cumulus plagioclase decreases.

The felsic intrusion

The quartz diorite samples are metaluminous, with values of alumina saturation index [(ASI: molecular $Al_2O_3/(CaO + Na_2O + K_2O)$] ranging from 0.91 to 1 (Table 3). The tonalite to trondhjemite samples are metaluminous to marginally peraluminous with ASI values from 0.87 to 1.16 (Table 3). In the total alkalies

Table 2 Comparison of results of various Al-in-hb geobarometric calibrations for representative analyses of hornblende from the tonalitic and gabbroic sample of the Demirkent intrusive complex, Yusufeli area, Eastern Turkey

Analysis	Rim	Centre	Rim	Centre	Centre	Rim	Rim	Centre	Rim	Rim	Centre
Al pfu	0.93	1.15	1.06	1.21	1.23	0.87	1.11	1.18	0.98[a]	1.02[a]	1.33[a]
Estimated temperature	Estimated pressure (kbar)										
Blundy and Holland (1990)	Anderson and Smith (1995)										
At 700°C (T=800°C[b])	1.2	2.2	1.8	2.5	2.8	0.9	2.1	2.4	1.3	1.5	2.9
At 725°C (T=825°C[b])	0.96	1.9	1.7	2.2	2.5	0.7	1.8	2.1	1.0	1.2	2.6
At 750°C (T=850°C[b])	0.6	1.6	1.2	1.8	2.1	0.3	1.4	1.7	0.6	0.8	2.1

Al pfu Aluminum per formula unit
[a]Hornblende analysis from a gabbroic sample
[b]Crystallization temperature for the gabbroic sample

Table 3 Bulk-rock compositions of the mafic and felsic intrusive phases of the Demirkent intrusive complex

Sample (wt%)	G499	G503	G504	G515	G518	G607	G612	G621	G624	G625	G630	G633
SiO_2	50.17	47.35	48.31	57.5	47.07	46.88	46.4	50.57	52.26	54.65	54.23	49.06
TiO_2	2.34	0.22	0.42	0.78	2.54	0.22	0.75	2.32	0.78	0.72	0.93	0.73
Al_2O_3	15.3	22.66	21.4	17.46	15.92	22.88	20.56	14.9	18.7	17.91	18.38	15.71
Fe_2O_3	4.70	1.84	1.75	1.85	5.30	1.80	3.06	4.04	2.11	2.61	2.82	2.37
FeO	7.87	3.22	3.90	3.29	9.08	3.17	4.70	8.53	4.67	4.40	4.66	6.25
MnO	0.2	0.07	0.09	0.09	0.19	0.08	0.12	0.19	0.11	0.17	0.13	0.15
MgO	4.0	5.41	5.29	3.55	4.64	5.79	6.11	4.75	6.06	5.34	3.81	8.15
CaO	6.78	15.08	14.28	6.61	8.7	12.97	12.85	7.91	8.73	7.62	7.51	11.3
Na_2O	4.19	1.9	2.08	5.73	3.49	1.56	2.28	4.29	3.43	3.58	3.86	2.9
K_2O	0.56	0.08	0.1	0.68	0.58	0.81	0.1	0.36	0.65	0.95	1.26	0.13
P_2O_5	1.42	0.01	0.01	0.1	0.06	0.04	0.03	0.25	0.23	0.1	0.21	0.06
LOI	2.2	2.0	2.1	1.3	1.3	2.9	2.0	1.2	2.1	1.8	2.1	3.2
Mg#	0.34	0.63	0.58	0.52	0.34	0.65	0.56	0.36	0.56	0.55	0.45	0.57
(ppm)												
Rb	6.5	1.6	5.3	11	9.0	2.0	4.0	8.0	17.8	8.1	24.4	6.0
Ba	142	40	97.2	279	141	199	29	133	139.2	151.7	227	48
Th	2.8	0.1	0.2	NA	1.0	0.4	NA	2.2	2.2	8.0	1.9	NA
U	1.2	0.05	0.06	NA	0.2	0.1	NA	0.3	0.4	1.2	0.5	NA
Nb	3.5	0.3	0.5	7.0	4.3	1.0	3.0	5.0	2.3	5.5	3.3	4.5
Ta	0.1	0.06	0.05	2.0	0.2	0.25	1.2	0.35	0.1	0.4	0.2	1.0
Pb	NA	10.5	34.9	NA	3.1	NA	NA	NA	4.8	37.9	5.0	NA
Sr	225	249.9	211.6	285	252.2	377	299	248	166.1	217	249.7	141
Zr	97	6.8	12.6	110	54.1	10	12	209	51.1	127.5	115.6	42
Hf	3.0	0.2	0.3	NA	1.6	0.4	NA	4	1.5	3.0	3.0	NA
Y	26	5.2	6.4	25	23	10	10	38	20.1	22	31.2	11
Ce	38	2.2	3.6	42	13	5.0	25	42	19.5	39.5	23.5	35
Cr	12	103	92	27	14	230	89	51	103	38	21	137
Ni	20	144.8	51.4	20	0.4	35	48	41	55.7	1.9	6.6	50
Sc	18	27	19	13	33	23	24	28	35	17	30	34
K/Rb	715	415	157	513	535	3202	208	360	303	974	429	180
Rb/Sr	0.03	0.01	0.03	0.04	0.04	0.01	0.01	0.03	0.11	0.04	0.10	0.04
Sr/Y	8.70	48.1	33.1	11.4	11.0	37.7	29.9	6.50	8.30	9.90	8.00	12.8
La	17	1.0	1.6	NA	5.3	2.0	NA	18	8.9	21.2	10.9	NA
Ce	38	2.2	3.6	NA	13	5.0	NA	42	19.5	39.5	23.5	NA
Pr	NA	0.32	0.49	NA	1.77	NA	NA	NA	2.34	4.34	3.03	NA
Nd	27	1.7	2.6	NA	9.7	5.0	NA	23	10.5	18	15.7	NA
Sm	6.1	0.5	0.8	NA	2.5	0.7	NA	5.9	2.3	3.2	4.1	NA
Eu	2.4	0.39	0.36	NA	1.12	0.5	NA	2.2	0.83	0.85	1.24	NA
Gd	NA	0.82	1.04	NA	3.44	NA	NA	NA	2.74	3.22	4.65	NA
Tb	1.3	0.13	0.18	NA	0.59	0.5	NA	1.5	0.43	0.51	0.82	NA
Dy	NA	0.93	1.06	NA	3.6	NA	NA	NA	2.92	2.94	4.99	NA
Ho	NA	0.18	0.23	NA	0.78	NA	NA	NA	0.65	0.71	1.04	NA
Er	NA	0.55	0.61	NA	2.16	NA	NA	NA	1.78	2.03	3.26	NA
Tm	NA	0.08	0.09	NA	0.32	NA	NA	NA	0.33	0.34	0.43	NA
Yb	3.9	0.49	0.59	NA	2.23	0.6	NA	5.5	2.16	2.58	3.07	NA
Lu	0.6	0.07	0.08	NA	0.28	0.08	NA	0.87	0.31	0.41	0.46	NA
La_n/Lu_n	2.94	1.48	2.08	–	1.97	2.60	–	2.15	2.98	5.37	2.46	–
La_n/Yb_n	4.36	1.37	1.83	–	2.40	3.33	–	3.27	2.78	5.55	2.40	–
Eu/Eu*	1.13	1.85	1.21	–	1.17	0.99	–	0.98	1.01	0.802	0.87	–

Sample (wt%)	G635	G681	G681B	G683	G694	G884	G908	G909	T420	T502	T614	T615
SiO_2	57.81	50.81	49.9	47.63	47.89	48.37	47.46	45.42	73.59	75.72	70.69	70.85
TiO_2	1.61	0.29	0.28	0.54	0.30	0.89	1.20	0.42	0.29	0.13	0.37	0.36
Al_2O_3	16	19.81	19.28	23.47	19.91	16.17	21.56	18.3	12.95	12.44	14.37	14.08
Fe_2O_3	1.66	1.76	2.35	2.40	1.74	3.08	3.63	4.35	1.47	0.95	0.33	0.94
FeO	6.42	3.44	3.11	3.25	3.06	5.71	5.14	6.25	2.11	2.02	2.93	2.32
MnO	0.13	0.1	0.1	0.09	0.09	0.12	0.2	0.2	0.04	0.04	0.06	0.1
MgO	2.87	7.24	7.44	4.89	9.12	9.3	4.63	9.93	0.98	0.12	0.77	0.7
CaO	7.51	12.71	13.37	13.91	15.09	11.22	9.67	10.66	0.74	0.64	2.41	2.62
Na_2O	5.3	2.6	2.43	2.14	1.35	2.48	3.66	1.46	5.83	6.23	4.88	4.8
K_2O	0.24	0.11	0.07	0.1	0.19	0.42	0.33	0.4	0.17	0.07	1.57	1.61
P_2O_5	0.23	0.01	0.01	0.02	0.01	0.03	0.49	0.05	0.01	0.01	0.02	0.12
LOI	0.7	1.7	1.4	1.2	1.9	1.9	1.8	2.5	0.8	0.8	1.3	1.3

Table 3 (Contd.)

Sample (wt%)	G635	G681	G681B	G683	G694	G884	G908	G909	T420	T502	T614	T615
Mg#	0.31	0.68	0.71	0.60	0.75	0.62	0.47	0.61	0.32	0.06	0.21	0.23
ASI	–	–	–	–	–	–	–	–	1.46	1.08	1.02	0.98
(ppm)												
Rb	13.4	3.0	0.1	2.4	3.9	10.7	7.0	4.0	30	24.1	37	35.9
Ba	3.9	1.6	34	37	55.4	111	176	106	90	8.0	349	382
Th	0.15	1.7	1.2	0.07	0.07	0.3	NA	NA	8.7	9.9	7.3	4.98
U	11	3.0	0.1	0.02	0.02	0.2	NA	NA	2.2	1.9	0.4	0.9
Nb	2.0	0.15	1.0	0.6	0.3	1.9	2.0	2.5	9.0	7.5	7.0	8.0
Ta	0.3	0.1	0.1	0.03	0.06	0.2	0.35	0.2	2.0	2.0	0.4	0.2
Pb	6.6	6.9	7.3	0.5	7.6	6.1	NA	NA	NA	NA	NA	NA
Sr	207	212	248	264	156	213	603	296	49	15	114	125
Zr	355	43	16	16	8.9	39	115	6.0	466	410	128	90
Hf	4.7	0.6	0.7	0.4	0.3	1.3	NA	NA	12	13	5.0	3.86
Y	45	9.0	11.3	7.4	6.7	15.5	15	7.0	46	49	17	20.4
Ce	20	160	7.1	4.0	7.3	7.2	12	10	72	81	69	31.8
Cr	14	160	96	151	438	89	41	144	24	22	10	8.0
Ni	20	35	22.3	18.8	103	38	41	32	< 10	1.4	< 10	1.8
Sc	17	4.0	41	29	35	34	21	28	4.0	2.0	8.0	1.3
K/Rb	149	261	5811	346	404	326	457	830	47.0	24.2	352	372
Rb/Sr	0.06	0.02	0.00	0.01	0.03	0.05	0.01	0.01	0.61	1.60	0.32	0.29
Sr/Y	4.40	21.2	22.0	35.7	23.2	13.8	40.2	42.3	1.07	0.31	6.71	6.11
La	23	9.0	3.3	1.9	1.3	3.9	NA	NA	42	50	20	17.9
Ce	42	160	7.1	4.0	2.9	8.5	NA	NA	91	100	36	31.8
Pr	5.34	NA	0.89	0.57	0.38	1.07	NA	NA	NA	10.96	NA	3.95
Nd	25	2.1	3.9	3.2	1.9	6.0	NA	NA	44	46	16	13.44
Sm	7.0	1.0	1.2	0.9	0.7	2.0	NA	NA	9.2	11	2.9	3.19
Eu	2.1	0.5	0.47	0.55	0.36	0.91	NA	NA	1.6	2.0	0.9	0.89
Gd	9.18	NA	1.47	1.07	1.01	2.23	NA	NA	NA	9.07	NA	2.77
Tb	1.7	0.3	0.28	0.21	0.16	0.47	NA	NA	2.1	2.2	0.5	0.76
Dy	12.19	NA	1.65	1.31	1.12	2.64	NA	NA	NA	13.7	NA	3.21
Ho	1.91	NA	0.37	0.27	0.22	0.58	NA	NA	NA	2.29	NA	0.67
Er	8.21	NA	1.03	0.8	0.62	1.59	NA	NA	NA	9.21	NA	2.34
Tm	1.21	NA	0.15	0.1	0.1	0.23	NA	NA	NA	1.42	NA	0.4
Yb	7.8	1.2	1.06	0.68	0.59	1.52	NA	NA	11.5	11.3	3.5	2.09
Lu	1.19	0.22	0.14	0.12	0.08	0.22	NA	NA	1.57	1.51	0.51	0.37
La_n/Lu_n	2.06	1.89	2.45	1.64	4.67	1.46	–	–	2.78	3.44	4.07	5.02
La_n/Yb_n	1.99	3.33	2.10	1.89	1.49	1.73	–	–	2.47	2.99	3.86	5.79
Eu/Eu*	0.80	1.21	1.08	1.71	1.31	1.31	–	–	0.92	0.60	1.65	0.90

Sample (wt%)	T619	T620	T622	T631	T632	T653	T654	T655	T677	T678	T689	T691
SiO_2	72.86	72.17	67.95	69.97	74.2	60.73	61.01	60.94	72.84	69.7	63.55	58.52
TiO_2	0.33	0.30	0.40	0.39	0.21	0.66	0.67	0.61	0.20	0.34	0.50	0.72
Al_2O_3	13.65	13.84	14.07	14.29	13.64	16.75	17.1	17.01	13.78	14.82	16.17	19.72
Fe_2O_3	0.77	0.72	1.04	0.93	0.71	2.64	2.46	2.75	0.51	0.64	2.34	2.21
FeO	2.47	1.95	2.21	2.66	1.45	4.16	4.08	3.90	1.61	2.57	3.83	3.61
MnO	0.05	0.09	0.07	0.08	0.03	0.14	0.16	0.16	0.06	0.07	0.11	0.12
MgO	0.55	0.54	0.88	0.94	0.49	2.31	2.37	2.42	0.36	0.68	2.13	1.87
CaO	1.95	2.98	3.32	2.86	1.82	6.09	5.98	6.06	1.83	2.7	5.39	7.32
Na_2O	4.83	5.4	5.69	4.52	5.51	3.87	3.55	3.52	5.39	5.43	3.26	3.72
K_2O	1.51	0.36	0.74	1.24	0.49	0.82	0.7	0.63	1.23	0.38	0.96	0.85
P_2O_5	0.02	0.09	0.07	0.03	0.06	0.15	0.1	0.09	0.07	0.06	0.08	0.14
LOI	1.2	1.4	4.1	1.1	1.2	1.4	1.0	1.4	2.4	1.6	0.9	1.7
Mg#	0.18	0.22	0.28	0.26	0.25	0.36	0.37	0.38	0.18	0.21	0.36	0.34
ASI	1.04	0.94	0.87	1.02	1.06	0.91	0.98	0.97	1.02	1.04	1.0	0.97
(ppm)												
Rb	34	6.52	20	26	9.57	11.57	8.0	8.65	18	16	8.0	10
Ba	450	231	82	307	106	262	221	146	208	179	228	198
Th	7.7	6.09	6.2	NA	7.9	1.8	NA	1.8	9.6	NA	NA	1.9
U	2.3	1.1	0.5	NA	1.5	0.2	NA	0.26	1.7	NA	NA	0.31
Nb	11	11	2.5	4.21	3.6	2.8	3.6	2.6	3.6	6.5	3.2	4.5
Ta	0.6	0.6	1.0	0.35	0.3	0.2	0.3	0.18	1.0	0.3	0.15	0.25
Sr	112	160	71	110	144	192	190	200	84	169	156	222

Table 3 (Contd.)

Sample (wt%)	T619	T620	T622	T631	T632	T653	T654	T655	T677	T678	T689	T691
Zr	233	122	120	110	79	53	69	80	113	139	72	59
Hf	7.0	4.99	4.0	NA	1.1	2.58	NA	3.0	4.0	NA	NA	2.0
Y	28	34.3	12	12	15	26.7	19	20	15	16	16	19
Ce	41	64.7	22	50	29	19.1	27	21	44	50	25	22
Cr	14	7.0	30	50	18	30	50	40	20	40	50	30
Ni	< 10	1.1	< 10	< 10	3.6	6.2	< 10	< 10	< 10	< 10	< 10	< 10
Sc	6.0	1.4	6.0	10	7.0	19	19	19	3.0	10	13	18
K/Rb	369	458	307	396	425	588	709	605	567	197	978	697
Rb/Sr	0.3	0.04	0.28	0.3	0.07	0.06	0.04	0.04	0.21	0.09	0.05	0.05
Sr/Y	4.0	4.6	5.9	9.2	9.6	7.2	10.0	10.0	5.6	10.5	9.7	11.7
La	21	37.4	10	NA	15	10.3	NA	9.0	24	NA	NA	9.0
Ce	41	64.7	22	NA	29	19.1	NA	21	44	NA	NA	22
Pr	NA	8.14	NA	NA	10	2.64	NA	NA	NA	NA	NA	NA
Nd	15	26.91	8.0	NA	3.28	11.35	NA	11	17	NA	NA	9.0
Sm	3.6	5.62	1.9	NA	1.88	3.34	NA	2.8	2.7	NA	NA	2.9
Eu	1.1	1.03	0.6	NA	0.71	1.1	NA	0.9	0.7	NA	NA	1.1
Gd	NA	4.81	NA	NA	2.29	3.39	NA	NA	NA	NA	NA	NA
Tb	0.8	1.23	0.5	NA	0.4	0.94	NA	0.35	0.5	NA	NA	0.6
Dy	NA	5.49	NA	NA	2.37	4.31	NA	NA	NA	NA	NA	NA
Ho	NA	1.09	NA	NA	0.47	0.88	NA	NA	NA	NA	NA	NA
Er	NA	3.84	NA	NA	1.74	3.01	NA	NA	NA	NA	NA	NA
Tm	NA	0.63	NA	NA	0.23	0.48	NA	NA	NA	NA	NA	NA
Yb	5.9	3.59	2.5	NA	1.68	2.71	NA	3.5	3.0	NA	NA	3.3
Lu	0.91	0.58	0.44	NA	0.26	0.43	NA	0.57	0.5	NA	NA	0.54
Eu_n/Eu^*	1.62	0.59	1.68	–	1.05	0.99	–	1.71	1.38	–	–	2.01
La_n/Lu_n	2.40	6.69	2.36	–	5.99	2.49	–	1.64	4.98	–	–	1.73
La_n/Yb_n	2.41	7.04	2.70	–	6.03	2.57	–	1.74	5.41	–	–	1.84

Mg# = MgO/(MgO + FeO), Eu* = (Sm + Gd)/2, *G* gabbro-diorite samples, *T* tonalite-trondhjemite samples, *NA* non analysed

versus silica diagram (Fig. 4c), while the samples of small intrusion fall into the field of diorite, the samples of the larger intrusion fall into the fields of quartz diorite and granodiorite; with their subalkalic characters (Wilson 1989). K_2O contents range between 0.07 and 1.61 wt%. On the SiO_2–K_2O variation diagram (Fig. 4a), the samples plot commonly in the field of low-K tholeiitic series (Peccerillo and Taylor 1976). The rocks have low MgO (2.0–2.4 wt%) contents and Mg-numbers [MgO/(MgO + FeO)] ≤ 0.38 (Table 3) and exhibit a calc-alkaline character on the A–F–M diagram (Fig. 5) (Irvine and Baragar 1971). On a normative An–Ab–Or diagram (Fig. 8), while the small intrusion samples plot in the tonalite field, the larger intrusion samples plot in the trondhjemite field of Barker (1979). A distinctive feature of the felsic intrusive rocks is that they contain relatively high concentrations of Na_2O, to as much as 6.23 wt%. On a K_2O–Na_2O–CaO diagram (Fig. 9a), the samples are characteristically scattered along the trondhjemitic trend line (Barker and Arth 1976). Their Na enrichments relative to Ca and K are similar to those of Archean tonalites, trondhjemites and dacites (TTD) believed to be derived from partial melting of metamorphosed basalt (Martin 1987). This is in strong contrast to the typical calc-alkaline differentiation trend of most arc suites. A similar distribution is shown on a normative Q–Ab–Or ternary diagram (Barker and Arth 1976) (Fig. 9b). This differentiation trend is also corroborated by the petrographic results, which show the low-K trondhjemitic trend of Lameyre and Bowden (1982) on the Q–A–P diagram (Fig. 3). Most of the variation diagrams (Fig. 4) show a straight line variation of elements with SiO_2, implying that the trondhjemites were evolved from the tonalites mainly by fractionation processes.

The investigated rocks are characterized by the following ranges in incompatible element contents and ratios: Rb 7–36 ppm; Sr 15–222 ppm; K/Rb = 24–978; Rb/Sr = 0.04–1.6; Sr/Y = 1–12. The average K/Rb value of 484 is higher than that of the upper continental crust ratio of 250 (Taylor and McLennan 1985) (Fig. 10a). On a Sr–Rb variation diagram (Fig. 10b), the felsic intrusive rocks are characterized by high Sr and Rb contents, and by moderately high Rb/Sr ratios relative to oceanic plagiogranites of Coleman and Peterman (1975). It is also clear that the bulk of quartz diorites have higher Rb/Sr ratios, of an average of 0.04, and differentiate to higher Rb/Sr values towards the tonalite and trondhjemite, which overlap, in part, the field of continental trondhjemite. Only two samples contain Rb/Sr values above 1 and represent the most evolved rocks of the intrusion. The low Sr and high Y signature of the samples is illustrated in Fig. 11 (Defant and Drummond 1993). All the samples plot in the field of island arc (ADR). In contrast to Archean high-Al TTD, the quartz diorite samples, which are the least fractionated products of the unit, have high Y (16–26 ppm) and low Sr/Y (7–11) values and evolved to higher Y and lower Sr/Y values towards the tonalites and trondhjemites.

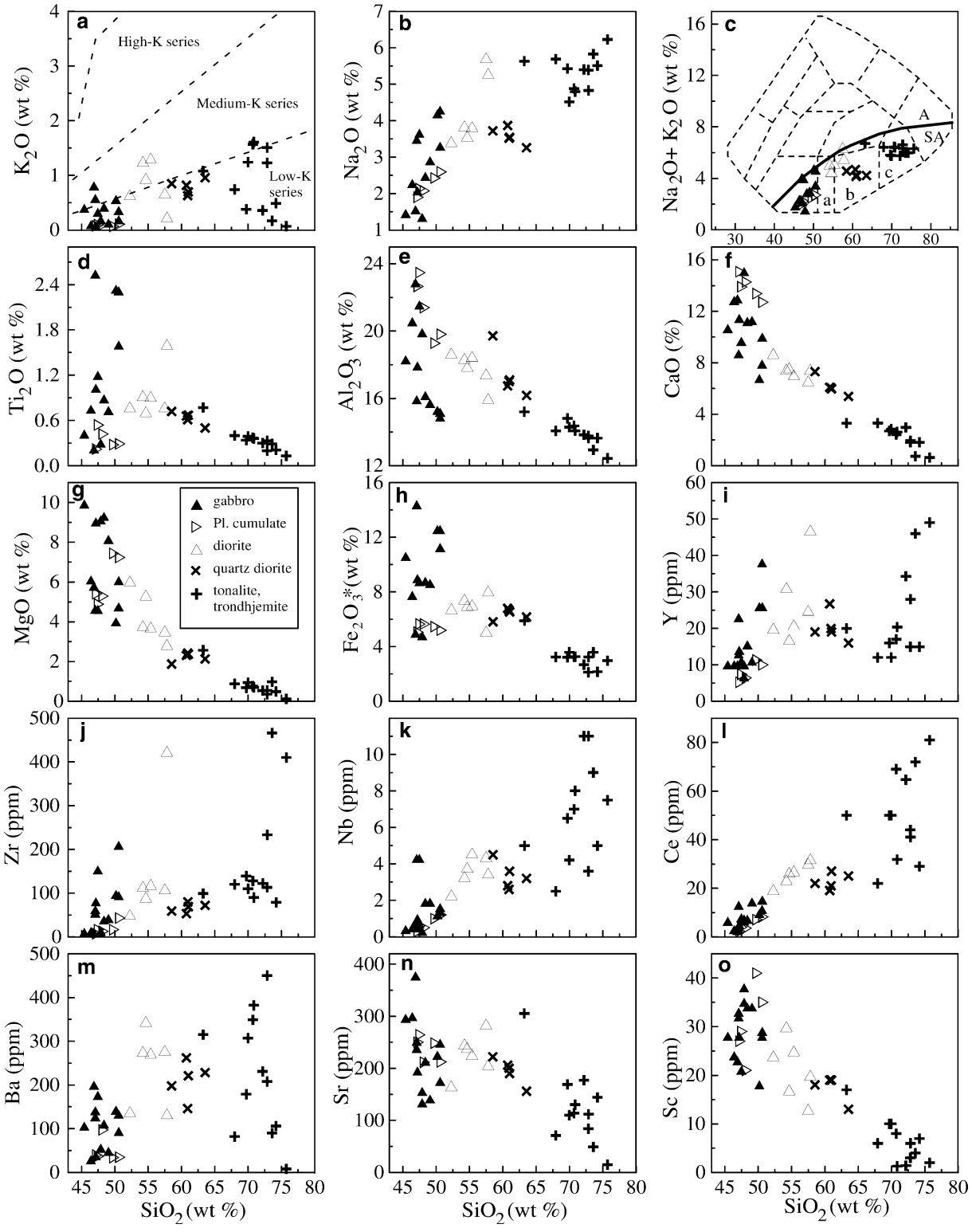

Fig. 4 a–o Harker variation diagrams for the samples from the Demirkent intrusive complex. The boundary lines for low-, medium- and high-K series are from Peccerillo and Taylor (1976). The diagram of (**c**) of total alkali versus silica variation on which the *curved solid line* subdivides alkalic (*A*) from subalkalic (*SA*) rocks and the boundary lines for plutonic rocks (**a** gabbro, **b** diorite, and **c** quartz diorite, granodiorite) adapted from Wilson (1989)

The REE patterns for quartz diorite and tonalite-trondhjemite are not much different (Fig. 7b). They are all slightly enriched in LREE ($La_n/Lu_n = 2–7$). The REE enrichment factor is increased from quartz diorite (20× chondrite) to tonalite and trondhjemite (100× chondrite), with distinctly positive Eu anomalies (Eu/

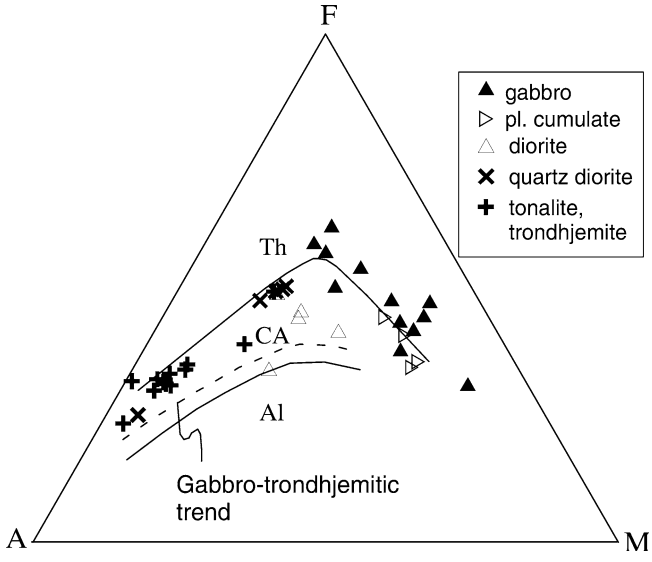

Fig. 5 A–F–M diagram showing tholeiitic to calc-alkaline trend for the mafic intrusive rocks and calc-alkali trend for the felsic intrusive rocks of the complex from the Yusufeli area (Irvine and Baragar 1971). Evolved rocks of the large felsic intrusion plot close to the felsic end of trondhjemitic trend of Barker and Arth (1976)

Eu* = 1.6–2.0) to moderately negative Eu anomalies (Eu/Eu* = 0.99–0.59), respectively. The REE pattern slope is nearly flat and the Eu anomaly deepens with fractionation.

Discussion

Inferred geological setting

The geological setting, the rock association, the mineralogy and the chemical composition of the rock types within the intrusive complex, all support the hypothesis that the igneous activity in the Yusufeli area occurred above an active subduction zone. The geological setting indicates a continental environment because mafic and felsic magmas intruded into the continental crust represented by various gneisses and schists (Dokuz 2000). However, the composite character and linear map patterns of the mafic and felsic intrusions, the common occurrences of hornblende-rich lithologies and the contemperaneous tonalitic to trondhjemitic magmatism distinguish the intrusions of the Demirkent intrusive complex from Alpine-type, ophiolitic bodies and stratiform layered intrusions in stable cratonic settings. The Demirkent intrusive complex far more resembles Alaskan-type bodies, such as those found in Sierra Nevada in California (Snoke et al. 1981) and Alaska (Irvine 1974).

The Alaskan-type intrusions of the Sierra Nevada are deeper parts of a volcanic arc, which formed at a convergent plate boundary (Davis et al. 1978). The chemical compositions also indicate that the mafic and felsic magmas of the Demirkent intrusive complex resemble those building up the Alaskan-type intrusions and they were formed above a subduction zone. The felsic intrusive rocks follow a low-K calc-alkaline trend towards trondhjemitic compositions, which has also been observed in Alaskan-type complexes (Snoke et al. 1981). Sr, K, Rb, Ba and Th (LILE) contents of the mafic and felsic intrusive rocks are enriched above MORB and ORG level (Fig. 12), probably indicating the contribution to the mantle wedge from dehydrated subducted-oceanic crust (Pearce 1983; Pearce et al. 1984). Gabbroic samples show a lesser degree of enrichment for the immobile (HFS) elements compared to MORB, presumably reflecting the pre-subduction characteristics of mantle wedge. High abundance of LILE relative to HFSE have been interpreted by many workers as the result of fluid enrichment processes related to the dehydration of the subducting slab (Gill 1981; Pearce 1983; Pearce and Peate 1995). Similar behaviour in trace element abundances and patterns can also be observed among the felsic rock types.

Indeed, such bimodal suites have been reported from a variety of environments closely linked to subduction zones: (1) intra-oceanic island arcs display variable volumes of mafic and felsic members (e.g. Meijer 1983;

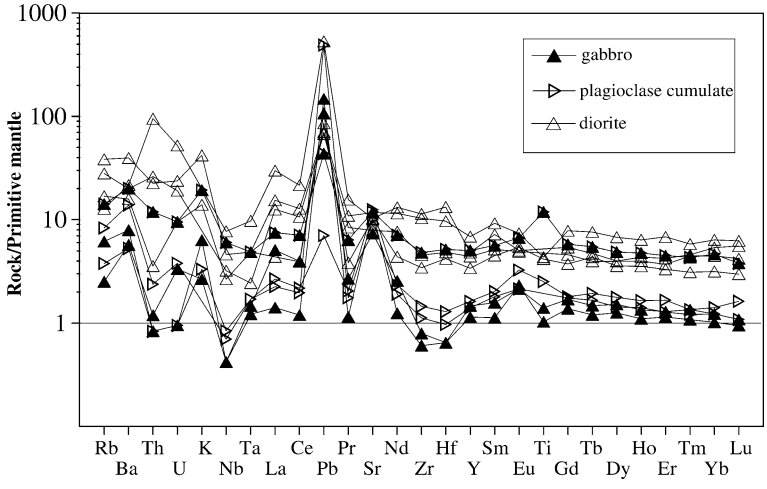

Fig. 6 Primitive mantle-normalized incompatible element spidergrams of the mafic intrusive rocks of the complex. Normalized values taken from Sun and McDonough (1989)

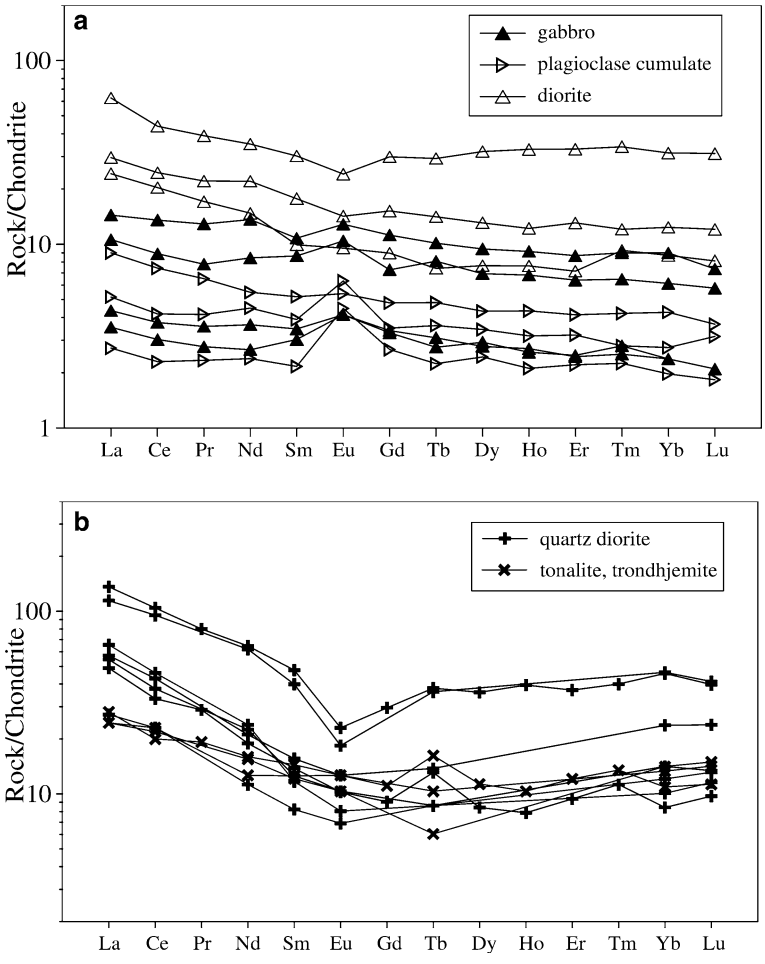

Fig. 7 **a**, **b** Chondrite-normalized plots showing the rare earth patterns for the mafic (**a**) and felsic (**b**) rocks of the complex from the Yusufeli area. The enrichment of the REE abundances increase within the samples from gabbros to diorites and tonalites to trondhjemites with increasing SiO_2. Abundances normalized to chondrites are from Taylor and McLennan (1985)

Brouxel et al. 1987), (2) mature island arcs, and volcanic arcs built on comparatively young or thin continental crust, are generally characterized by a predominance of andesites (e.g. Cascades, Grove and Donnelly-Nolan 1986; Central Chile, Frey et al. 1984; Japan, Notsu et al. 1987), (3) a back-arc basin environment is suggested in some cases by the chemical characteristics range between N-MORB and island-arc types (e.g. Saunders et al. 1980; Wood et al. 1981), but bimodal associations were produced by, in particular, arc rifting, during the initiation of back-arc spreading (Hochstaedter et al. 1990; Ohki et al. 1994).

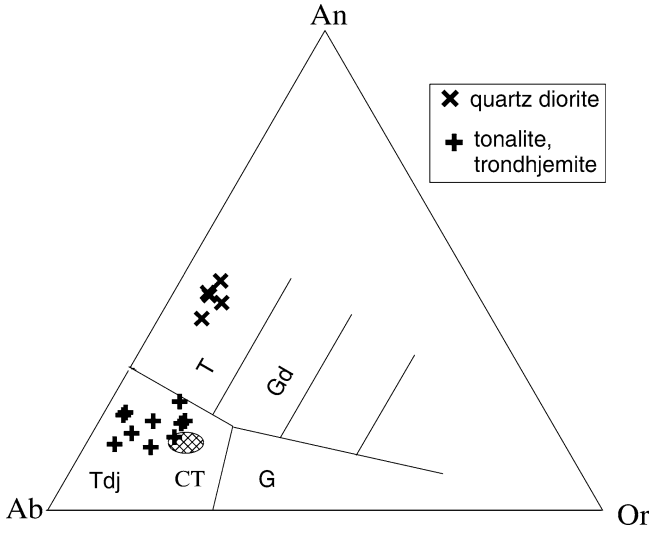

Fig. 8 Rock classification for the felsic part of the intrusive complex based on normative feldspar variation. The fields are those drawn by Barker (1979). *T* tonalites, *Gd* granodiorites, *G* granites, *Tdj* trondhjemites

Although the chemical characteristics of the rocks associated with the intra-oceanic island arcs fit rather well with the data obtained from the Demirkent intrusive complex, age constraints and field relations display more affinities with modern bimodal suites erupted during the early stages of rifting of magmatic arcs. The elongate map patterns of both the felsic and mafic intrusions and the presence of multiple dikes parallel to the long axis of the intrusions reflect the effects of extension during their emplacement. Early interpretations of the Demirkent intrusive complex as an ophiolite representing a fragment of oceanic crust formed at a spreading centre (Şengör et al. 1980; Adamia et al. 1995; Yılmaz et al. 1997) was based on the presence of dikes interpreted as sheeted and their low-K contents. More recent studies (Konak and Hakyemez 1996; Dokuz 2000), including this one, have shown important

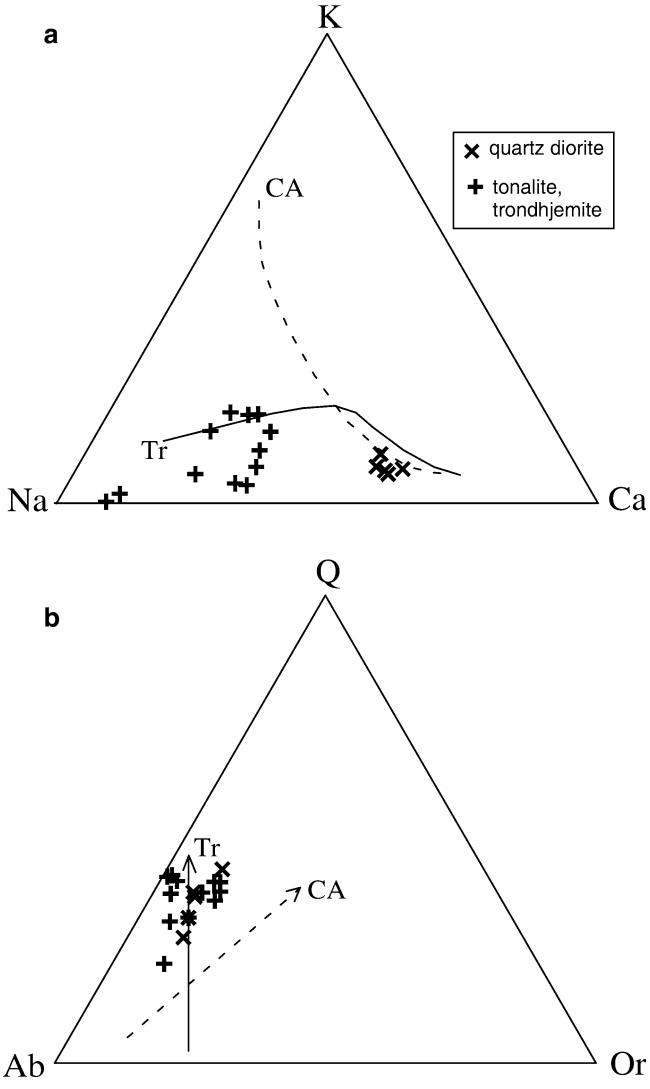

Fig. 9 **a**, **b** K–Na–Ca and normative Q–Ab–Or diagrams (Barker and Arth 1976) showing the trondhjemitic character of Early Jurassic felsic rocks of the intrusive complex. *Tr* trondhjemitic trend, *CA* calc-alkaline trend

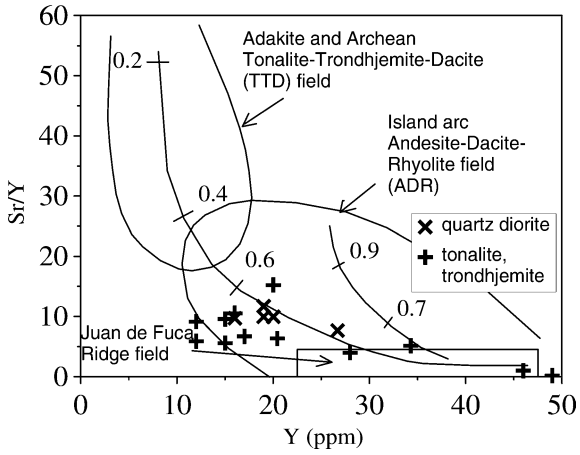

Fig. 11 Graph of Sr/Y versus Y of the Early Jurassic felsic intrusive rocks of the complex. Adakite and Archean high-Al TTD, island arc ADR, and Juan de Fuca Ridge fields are from Defant and Drummond (1993). Felsic igneous rocks of the complex plot in the field of island arc ADR and differentiate to lower Sr/Y and higher Y values, which is in the reverse direction with regard to those of derived from partial melting of oceanic crust

differences between the Demirkent intrusive complex and ophiolites. First, the felsic rocks of the complex are not plagiogranite and do not display a tholeiitic differentiation trend. Although there is a compositional gradation from mafic rocks to felsic rocks in Harker diagrams (Fig. 4), which is also an important feature of the plagiogranites, there is a clear-cut intrusive relation developed between the mafic and felsic rocks of the Demirkent intrusive complex. Besides, since the plagiogranites occurred as end-products of differentiation within ophiolite sequences, they occupy volumetrically small areas, such as small intrusive plugs or parallel dikes within diabase (Coleman and Peterman 1975). In contrast, the felsic rocks of the Demirkent intrusive complex cover a large area (22 km^2) enough not to be derived from the mafic rocks (exposed in the area of 30 km^2) by crystal fractionation.

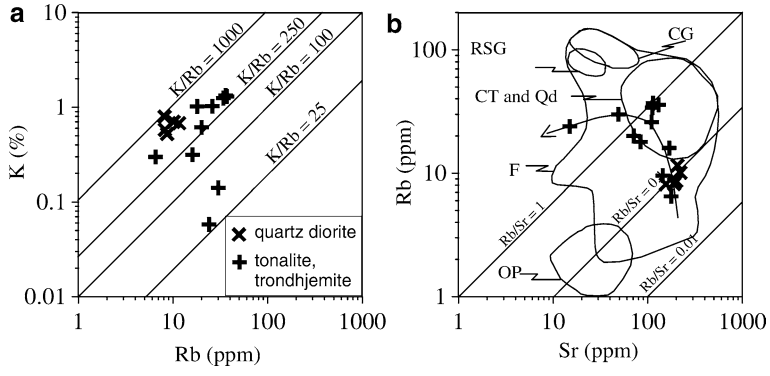

Fig. 10 **a**, **b** K versus Rb and Rb versus Sr variation diagrams for the felsic intrusive rocks of the Demirkent intrusive complex. In the K versus Rb diagram (**a**), the analyses mainly plot above the lines of average continental crust (K/Rb = 250) of Taylor and McLennan (1985). In the Rb versus Sr diagram (**b**), the felsic rocks of the complex plot in the field of island arc and continental margin calc-alkaline volcanic rocks (*F*). Other fields including oceanic plagiogranites (*OP*), continental trondhjemites and quartz diorites (*C T* and *Qd*), Red Sea granophyres (*RSG*), and continental granophyres (*CG*) are for comparison (after Coleman and Peterman 1975)

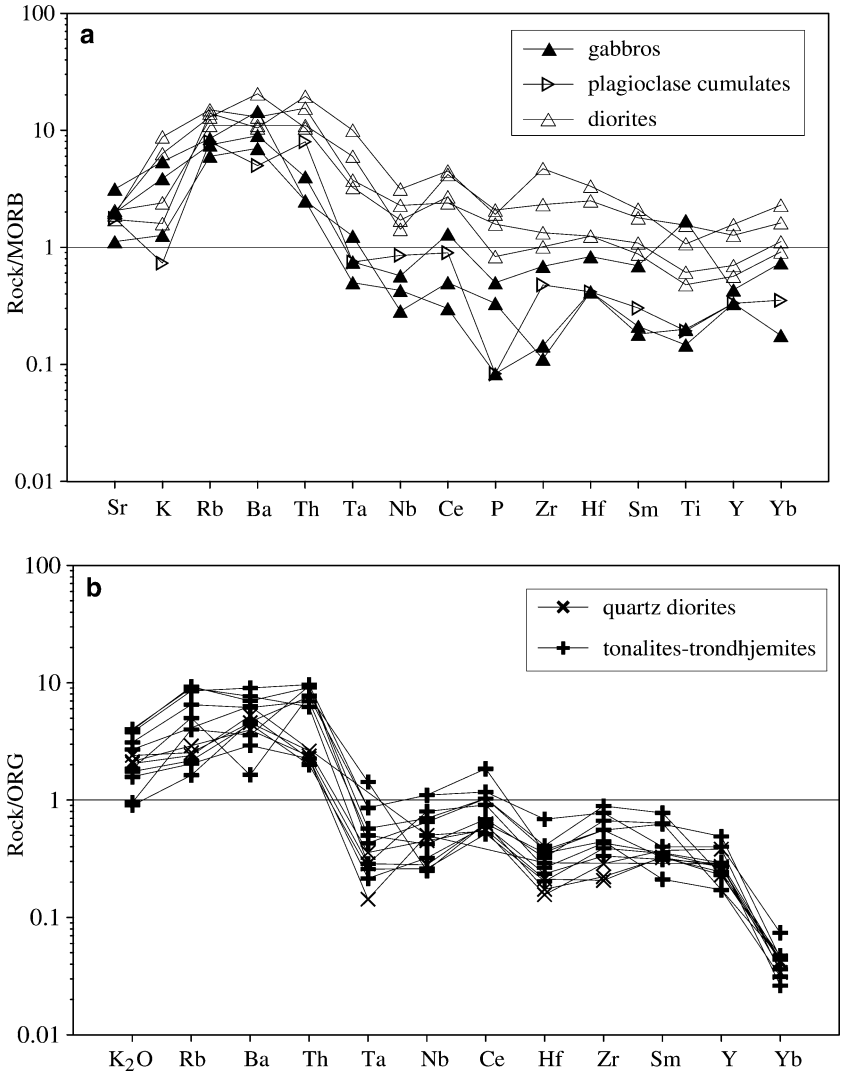

Fig. 12 **a**, **b** Oceanic ridge-basalt and -granite normalized diagrams showing representative samples from each of the intrusive units of the complex. MORB and ORG data are from Pearce (1983) and Pearce et al.(1984), respectively

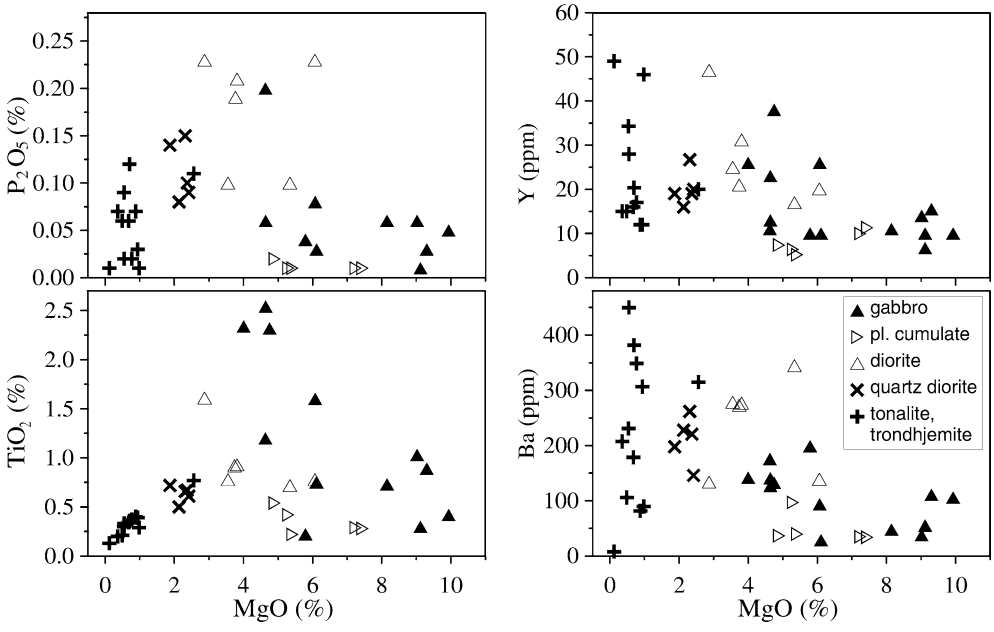

Fig. 13 MgO versus major and trace element variation diagrams for the selected elements showing different fractionating lines of each of the intrusive rocks forming the complex

Table 4 Major element oxides fractional crystallization modelling for the mafic and felsic rocks of the Demirkent intrusive complex

	Fractionated phases						
	G694[a]	Cpx.	Plag.	Hornb	G635[b]	Calculated	Residuals
SiO_2	48.5	50.59	50.40	50.76	58.07	57.79	0.282
TiO_2	0.30	0.87	0.00	0.93	1.62	1.76	−0.151
Al_2O_3	20.16	3.96	31.01	6.35	16.07	16.04	0.024
Fe_2O_3	4.86	7.10	0.30	11.56	8.12	8.26	−0.142
MnO	0.09	0.16	0.33	0.57	0.13	−0.275	0.404
MgO	9.24	12.84	0.00	17.77	2.88	2.80	0.081
CaO	15.28	24.06	14.75	11.60	7.54	7.54	0.002
Na_2O	1.37	0.42	3.21	0.45	5.32	5.58	−0.251
K_2O	0.19	0.00	0.00	0.00	0.24	0.49	−0.249
$\sum R^2$							0.417
Proportion (wt%) of a phases fractionated	23.65	3.2	40.72	32.43		76.35	
Percent solid		4.19	53.33	42.48			

	Fractionated phases							
	T653[c]	Plag.	Hornb.	Apt.	Mt.	T502[d]	Calculated	Residuals
SiO_2	62.09	53.06	50.93	0.60	3.71	76.97	76.866	0.11
TiO_2	0.62	0.01	1.19	0.00	2.99	0.13	0.394	−0.263
Al_2O_3	17.33	31.17	5.46	0.00	0.90	12.65	12.627	0.019
Fe_2O_3	6.78	0.27	14.76	0.00	89.18	3.02	2.903	0.121
MnO	0.16	0.03	0.50	0.05	0.0	0.04	0.091	−0.054
MgO	2.47	0.02	15.21	0.00	0.23	0.12	0.074	0.053
CaO	6.17	12.51	11.48	54.00	2.93	0.65	0.327	0.32
Na_2O	3.59	2.86	0.06	0.48	0.06	6.33	5.985	0.351
K_2O	0.64	0.06	0.42	0.00	0.00	0.07	0.59	−0.521
P_20_5	0.15	0.00	0.00	44.87	0.00	0.01	0.143	−0.135
$\sum R^2$								0.62
Proportion (wt%) of a phases fractionated	46.7	33.80	16.08	0.03	3.39		53.30	
Percent solid		63.42	30.17	0.05	6.36			

Note that the parents and daughters were recalculated to 100% and the total iron is given as Fe_2O_3. The composition of clinpyroxene, plagioclase, hornblende, magnetite and apathite are from Dokuz (2000).
[a]Gabbroic parent magma (clinopyroxene + plagioclase + hornblende) for the mafic rocks
[b]Selected representative daughter for the mafic rocks of the complex
[c]Quartz dioritic parent magma (hornblende + plagioclase + apathite + magnetite) for the felsic rocks
[d]Selected representative daughter for the felsic rocks of the complex

Parental magma composition

The mafic intrusion

The composition of the parental magma to the gabbroic rocks of the Demirkent intrusive complex can be estimated from the composition of most primitive non-cumulate gabbros and by comparison with crystallization sequences from experimental studies. The non-cumulate gabbros may be considered to represent near-liquid composition derived from melting of an upper mantle source.

The sample G694 is the most mafic non-cumulate gabbro and is thought to approach the parental magma composition with its Mg-number of 75.9, MgO, Cr and Ni contents (9.12 wt%, 438 and 103 ppm, respectively), REE abundance (~3× chondrite), flat REE-pattern (La_n/Lu_n(4.6), and a slightly positive Eu anomaly (Eu/Eu* = 1.31) (Wilson 1989). It has low Ni content relative to those of primitive unfractionated magmas (200–450 ppm; Frey et al. 1978), interpreted to result from some prior olivine or orthopyroxene fractionation. Also Al_2O_3 content (20 wt%) is not consistent with basaltic parent melt ($Al_2O_3 < 15$ wt%) in equilibrium with mantle source, likely because of the fractionation of some Al-poor mafic phases, such as olivine and orthopyroxene. However, the rare earth element data for the non-cumulate gabbros indicate that this fractionation could not have been much extensive because their REE patterns are slightly fractionated (Fig. 7a).

Most of the experimental parents from hydrous melting of olivine tholeiites at high pressures closely match the observed sequence in the gabbroic rocks of the Demirkent intrusive complex in terms of crystallization sequences, mineral composition and modes (Green 1982; Housh and Lurh 1991; Moore and Carmichael 1998). The absence of orthopyroxene and abundance of amphibole are the most important similarities between the likely parent for the mafic intrusive rocks and experimental melts under water-saturated conditions. Orthopyroxene is a common mineral in anhydrous basalt crystallization, but is replaced by

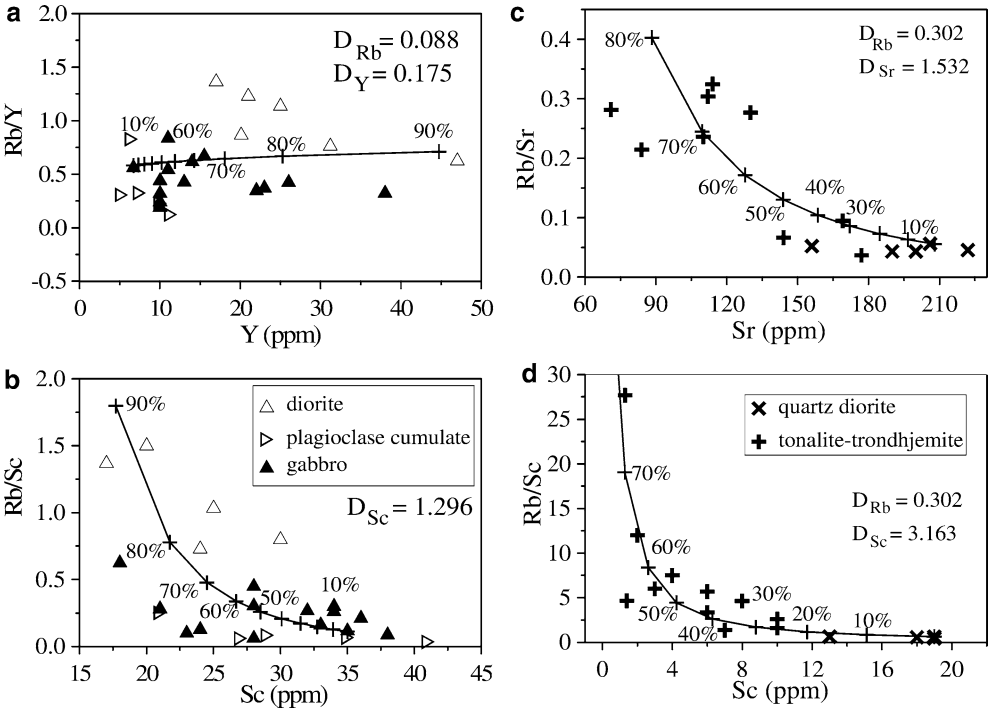

Fig. 14 Trace element fractional crystallization modelling of the Demirkent intrusive rocks. The diorite samples (**a**, **b**) of the mafic intrusive and the tonalite samples (**c**, **d**) of the felsic intrusive were produced, in turn, at 70–85 and 55–75 vol % fractional crystallization involving clinopyroxene, hornblende and plagioclase from a gabbroic magma, and hornblende, plagioclase, apatite and magnetite from a quartz dioritic magma

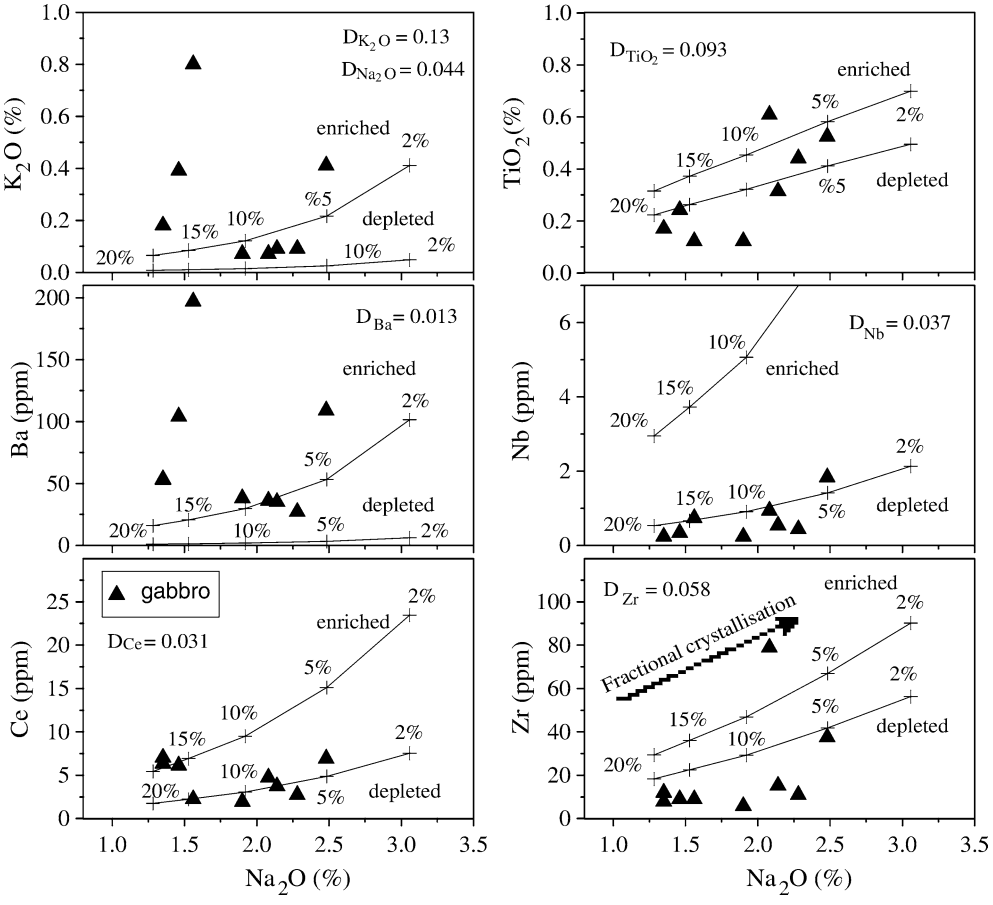

Fig. 15 Variation in large ion lithophile and light rare earth elements and high field strengh elements plotted against Na_2O for the most primitive mafic rocks of the gabbro-diorite body. *Curves* show non-modal batch partial melting models for depleted and enriched mantle source regions calculated using compositional data from Michael (1988). Mineral/melt partition coefficients used in the calculations of bulk partition coefficients (*D*) are compiled from Fujimaki et al. (1984) and Irving and Frey (1978). *D* (solid/melt) values are for a mantle source or residue comprising 60% olivine, 30% orthopyroxene and 10% clinopyroxene. Bulk distribution coefficients (*P*) of minerals making up the melt of 10% olivine, 30% orthopyroxene, and 60% clinopyroxene calculated by using same mineral/melt partition coefficients. *Curves* are marked in increments of 5% melting and show a maximum of 20% melting at *far left*

olivine, clinopyroxene and amphibole when water is present. Amphibole completely replaces pyroxene at the lowest temperature. Thus, the parents for the gabbroic rocks of the complex were apparently highly hydrous (~5–6 wt%), implying early fractionation of anhydrous phases, such as olivine and clinopyroxene and possibly

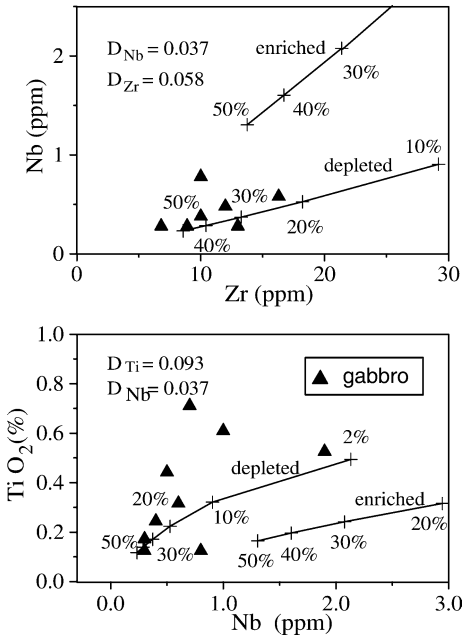

Fig. 16 Nb versus Zr and TiO_2 versus Zr for the most primitive tholeiitic mafic rocks of the Early Jurassic intrusive complex from the Yusufeli area. *Curves* show batch partial melting models for depleted and enriched mantle source regions as described in Fig. 13. Curves are marked in increments of 10% melting and show a maximum of 50 % melting at far left

orthopyroxene. With these guidelines, the parental magma must have been a partly fractionated, high-magnesian and high-aluminum tholeiite, rich in incompatible elements.

The felsic intrusion

On the variation diagrams of SiO_2 versus some major and trace elements (Fig. 4), the samples of the felsic intrusion fall on the same trend as samples of the mafic intrusion, which might imply that the felsic intrusive rocks were generated from the mafic rocks of the complex by fractional crystallization. This is supported by the modal mineralogical similarity between the most evolved rocks (diorites) of the mafic intrusion and the primitive or parental rocks (quartz diorites) of the felsic intrusion. However, on the diagrams of MgO versus some major and trace elements (Fig. 13), a clear discrimination between the differentiation trends of both the mafic and felsic intrusive rocks can be observed, indicating necessity of an additional process in the generation of the felsic rocks. Compositional scattering in Ba, Y and to a lesser extent P_2O_5 for the felsic rocks in Harker diagrams may result from combined effects of fractionation and assimilation, and, in part, may be an artefact of insufficient sampling for the primitive rocks of the large intrusion. Also, the lack of the negative Eu anomalies in the quartz diorites and tonalites, which are the least evolved rocks of the felsic intrusion, rule out the fractional crystallization from the dioritic rocks of the mafic intrusion, which show negative Eu anomalies. Further, the felsic intrusion has an obvious intrusive contact with the mafic intrusive rocks and includes common mafic xenoliths. The presence of reaction rims around the xenoliths indicates that wall-rock assimilation should have been efficient during the magmatic emplacement. All these data indicate a later and new parental melt for the felsic part rather than generation from the mafic rocks of the complex by fractional crystallization. In the light of these data, a quartz dioritic parental melt for the felsic part of the complex, is suggested as it is the least evolved member.

Crystal fractionation

Crystal fractionation was responsible for the generation of various evolved lithologies within each intrusion. Trend lines through data for the mafic and felsic intrusions suggest fractional crystallization as a possible cause for compositional variation within the intrusion (Fig. 4). Also, the rocks of both intrusions show similar REE patterns with a general increase of both the light and the heavy REE with increasing SiO_2 (Fig. 7). The magnitude of the negative chondrite-normalized Eu anomalies increases with increasing SiO_2 contents (Fig. 7), suggest crystallization of plagioclase for both the intrusions. Crystallization of plagioclase is also consistent with the decrease in abundances of Al_2O_3 and CaO (Fig. 4e, f) and the negative MORB-normalized Sr anomalies, which increase in magnitude with increasing SiO_2 content (Fig. 12). Crystallization of other minerals is also suggested by these geochemical data. Abundances of Sc (Ni and Cr) decrease with increasing abundances of SiO_2 (Fig. 4o) and decreasing abundances of MgO content (Table 3), suggesting Cr and Ni were compatible with the crystallizing minerals including clinopyroxene for the mafic intrusion and hornblende for the felsic intrusion. Abundances of Y also increase with increasing abundances of SiO_2 (Fig. 4i) and suggest the accumulation of amphibole for the mafic intrusion. Increasing TiO_2 (and P_2O_5) contents (Fig. 4d) and magnitutes of slightly negative to positive Ti and P MORB-normalized anomalies (Fig. 12) with increasing SiO_2 content may indicate accumulation of ilmenite, magnetite and apatite for the mafic intrusion, which accord with the modal calculations. As for the felsic intrusion, the trends of these elements are in reverse direction (Figs. 4d, 13), which may demonstrate fractionation of ilmenite, magnetite and apatite. These geochemical features together with their mineralogy are consistent with a genetic relationship between the least and most evolved products of both the intrusions. Considering all these data together, it is likely that fractional crystallization affected the magmas represented by Demirkent intrusive complex.

Crystal fractionation in the intrusions was modelled by using the least-squares mass balance calculations for the major elements as outlined by Stormer and Nicholls (1978). The composition of plagioclase, clinopyroxene,

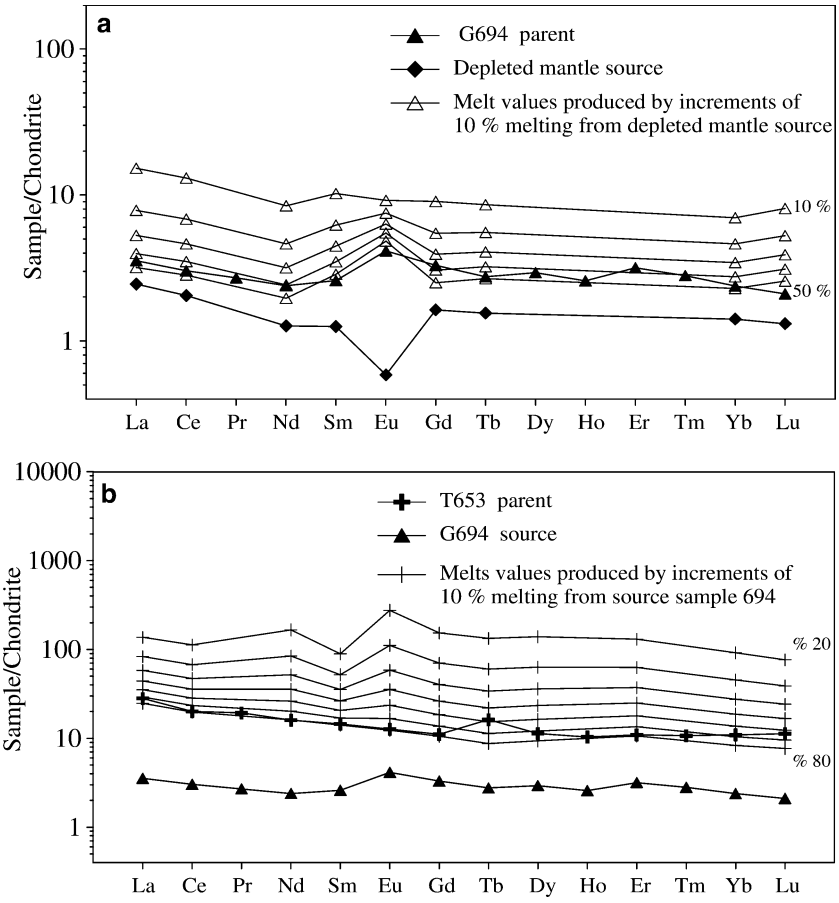

Fig. 17 **a**, **b** REE-normalized batch partial and fractional melting values to acquire the parents of each of the mafic and felsic intrusive rocks of the complex. In the diagram of (**a**), depleted mantle and least evolved sample of G694 are chosen as source and parent for the mafic intrusion, respectively. Depleted mantle source REE values are from Michael (1988). Mineral/melt partition coefficients used in the calculations of bulk partition coefficients (*D*) for the mafic intrusion are as described in Fig. 13. In the diagram of (**b**), the parent (G694) of the mafic intrusion is chosen as source for the felsic intrusion. The partition coefficients used for the felsic intrusion are collected from the references included in Rollinson (1993). The *lines* are marked in increments of 10% melting

hornblende and magnetite used in the models are microprobe analyses of minerals from the rocks of mafic and felsic intrusions. The results of these calculations are shown in Table 4. Most solutions given here have sums of squared residuals less than 1. The sample G694, a clinopyroxene-rich non-cumulate gabbro, is the most undifferentiated sample of the mafic intrusion that has the mineralogical and geochemical attributes of non-cumulate rocks. These include elevated incompatible element contents, flat LREE pattern and zoned plagioclase. It is also very mafic and alkali-poor, but is similar in composition to the most mafic arc basalts. The derivation of evolved diorites (G635) by fractional crystallization from the more basic magma (G694) was modelled. The model allows formation of evolved diorites by ~77% crystal fractionation (Table 4). The crystallizing mineral phases are dominated by clinopyroxene, plagioclase and hornblende, which constitute by ~99% of the mineralogy. The residual sum of squares is 0.41, indicating that predictions of the crystallizing mineral phases and their proportions were reasonable. The fractionation-derivation process was repeated for the felsic intrusion to produce a representative evolved rock composition (Table 4). The sample T653 and the sample T502 are chosen as parent and daughter, respectively. The trondhjemitic sample (T502) was produced succesfully form the tonalitic parent (T653) by a ~54% fractionation of plagioclase, hornblende, apatite and magnetite with residual sum of squares of 0.62. Fractionating proportions of minerals are shown in Table 4.

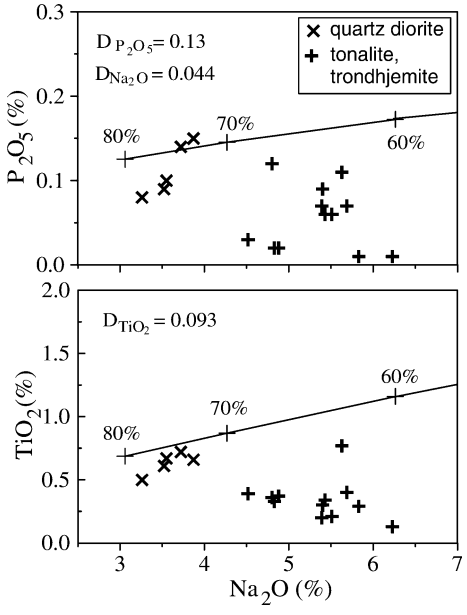

Fig. 18 Major element partial melting modelling of the felsic intrusive. The quartz diorite samples (*crosses*) were yielded at 70–80% partial melting from a gabbroic (G694) magma

Trace element fractional crystallization modelling supports the major element models. The Rb/Y versus Y and Rb/Sc versus Sc diagrams (Fig. 14a, b) suggest that evolved members of the mafic rocks require 70–87% fractional crystallization of 53% plagioclase, 43% hornblende and 4% clinopyroxene from the gabbroic sample, presumed to be representative of starting material. In the same way, derivation of fractionated materials of the felsic rocks from a quartz dioritic sample needs 50–65% fractional crystallization of 63% plagioclase, 30% hornblende, 6% magnetite and 0.05% apatite (Fig. 14c, d). The fractionation models demonstrate that crystal fractionation is a permissible mechanism for producing the range in rock compositions in the mafic and felsic intrusions of the Demirkent intrusive complex.

Considerations on the source compositions of the intrusions

The mafic intrusion

The mafic intrusive rocks of this study display a wide range of elements characteristic of mafic rocks such as MgO (9.12–2.87 wt%), Ni (159–20 ppm) and Cr (438–7 ppm). These characteristics generally suggest a variably fractionated melt derived from upper mantle source. Furthermore, higher LILE and lower HFSE concentrations relative to MORB indicate a mantle source that is enriched in the LILE relative to the HFSE (Fig. 12). Such a source is commonly invoked for subduction-related magmas (e.g. Pearce and Peate 1995) and is presumably located in the convecting asthenospheric mantle wedge above subducting slab (McCulloch and Gamble 1991; Stolper and Newman 1994).

Sample G694 has Mg-number and MgO content as high as 75 and 9.12 wt%, respectively, which would be consistent with the sub-continental lithospheric mantle (Wilson 1989). The flat chondrite-normalized REE patterns and low abundances of REE contents (approximately 3× chondritic) of the cumulate and non-cumulate rocks are typical for a moderate degree of melting of a garnet-free peridotitic mantle source. Undepleted HREE contents in the gabbroic rocks rule out the presence of residual garnet in the mantle source. Basaltic sources such as MORB and metamorphosed basalts can also be ruled out, because their partial melting gives rise to HREE-depleted magmas. Luais and Hawkesworth (1994) have demonstrated that there is no garnet in the residue at 8 kbar, and hence the melts would have flat HREE patterns. In contrast, the higher-pressure melts (22–32 kbar) are in equilibrium with an eclogite residue, and therefore have strongly fractionated REE patterns ($La/Yb_n = 18–47$) with low Yb contents ($Yb = 1.5$) (Luais and Hawkesworth 1994).

On the other hand, all the mafic rocks have alumina contents >15 wt% which increases up to 22 wt% with increasing MgO. This is inconsistent with the lower Al_2O_3 (<15 wt%) values of mantle-derived magmas. Similarly, parent rocks to the mafic intrusion have also enriched CaO contents, reaching upto 15 wt%, with respect to mantle-derived, primitive tholeiitic magmas. Derivation of such high-Al and Ca-bearing magmas from tholeiite would require significant fractionation of Al_2O_3- and CaO-poor mafic phases, in particular, olivine, as suggested by Perfit et al. (1980) and Kay et al. (1982). Partial melting experiments of hydrous peridotite indicate that Al_2O_3 concentrations decrease with increasing melt fraction, such that melts in equilibrium with a refractory source would have relatively low Al_2O_3 (Kushiro 1990; Hirose and Kawamoto 1995; Hirose 1997). This suggests that a mantle source region that has been depleted in Al during previous partial melting events would melt to yield relatively Al_2O_3−poor magmas. Similar behaviour would be shown by Ca if the previous partial melting was sufficient to remove clinopyroxene from the residual mantle assemblage (Tatsumi 1982). If such depletions had occurred in the mantle source, it should account for the anomalously low Al_2O_3 and CaO in the primitive tholeiitic mafic parent of the intrusive complex. In contrast, CaO and Al_2O_3 contents of primitive tholeiitic parent to the mafic rocks of the intrusive complex are higher than for primitive magmas, suggesting a small amount of melt fraction from the harzburgitic mantle. But, this interpretation is contradicted by the low REE abundances (3–6× chondritic) of parent rocks and partial melting models, which imply relatively an extensive partial melting. Hence, clinopyroxene-free (harzburgitic) mantle source cannot account for the formation of the parent to the mafic intrusive rocks. On the other hand, melts in equilibrium with refractory lherzolitic mantle have higher CaO and Al_2O_3 than those in equilibrium with a harzburgitic assemblage (Tatsumi 1982). Furthermore, the abundant Ca-bearing minerals, such as diopside, calcic amphibole and anorthitic plagioclase, in the parent rocks indicate a clinopyroxene-bearing (lherzolitic) mantle source.

In order to place constraints on the compositions of mantle source regions in which Early Jurassic tholeiitic magmas throughout the Eastern Pontides were generated, it is useful to compare the compositional data with partial melting models for various end-member mantle reservoirs. To illustrate this, batch partial melting models were carried out on source compositions varying from depleted to enriched lherzolitic mantle sources. The modal composition of mantle source is taken as lherzolite with the following mineralogy: olivine:orthopyroxene:clinopyroxene = 55:30:15. The geochemical compositions for the depleted and enriched mantle source regions are from Michael (1988). K_2O and Ba in the primitive tholeiitic rocks of the mafic intrusion are significantly greater than would be expected for melting of a depleted mantle source region (Fig. 15). In contrast, TiO_2, Zr, Nb and Ce concentrations for most of the rocks of the mafic intrusion scatter around the values predicted for melting of depleted mantle. These relations indicate a mantle source region for Early Jurassic

primitive tholeiitic magmas in the Yusufeli area that is enriched in the LILE relative to HFSE. Besides, the abundances of TiO_2, Zr, Nb and Ce in primitive magmas of the mafic rocks are consistent with the hypothesis that these magmas are generated from a mantle source region that has been depleted by previous partial melting events. The composition of parental gabbroic rocks fits best with 15–20% batch partial melting from a depleted lherzolitic mantle, consistent with the generally accepted degree of melting of about 20% or less for tholeiitic arc basalts and MORBs.

Inter-element ratios between HFSE in primitive tholeiitic magmas of the mafic intrusion are also consistent with the derivation from a depleted mantle source region (Fig. 16). However, in contrast to major element model, the calculated degree of partial melting varies from 40 to 50%, with an average of 45%. It is also favoured by the REE modelling, which indicates 40–50% partial melting to form primitive tholeiitic parent from the depleted mantle source (Fig. 17a). This contradiction may result from the higher HFSE and REE concentrations of assumed mantle source because such an extent of melting is highly model-dependant. Furthermore, as observed in the diagrams (Fig. 15), parent rocks plot on the lower side of the calculated line, indicating that depletion in HFSE in possible source would have more than those in the selected source. Absolute values of elemental abundances in the depleted mantle source used for the calculations are not nearly as well constrained as are the ratios of elements (e.g. Michael 1988).

The felsic intrusion

Based on the experimental, petrological and geochemical data presented in literature, possible mechanisms for the generation of silicic rocks are: (1) fractional crystallization from basaltic magma, (2) partial melting of immature greywackes, (3) direct partial melting of the mantle, (4) partial melting of basaltic source material, which has been transformed into either amphibolite, quartz eclogite or some transitional rock type.

As discussed earlier, the derivation from the mafic intrusive rocks by crystal fractionation process seems unsuitable. Moreover, if this process had worked during the generation of the felsic rocks, basic rocks would have been much more common relative to the felsics. The voluminous nature of the felsic rocks relative to the mafics in the study area (Fig. 2) argues against the formation of the felsic rocks by direct fractional crystallization from these mafic rocks. Melts directly derived from immature greywackes are also unsuitable due to the lack of these kinds of rocks in the basement represented by metamorphic rocks and granitoids. Low fraction partial melting of the mantle to yield magmas as felsic as dacite is unreasonable and is capable of yielding melts only as felsic as basaltic andesite, alkali basalt or boninite (Jahn et al. 1984). Low MgO concentrations of the samples of the felsic intrusion and other geochemical parameters rule out a direct derivation from mantle wedge. The lack of negative Eu anomalies in the least fractionated tonalites of the felsic intrusion—provided they represent unfractionated magma—reflects the absence of differentiation in terms of plagioclase exctraction in their parent melt. In order to evolve to a tonalite from mantle-derived basic parental magma would require a prominent fractionation, as discussed earlier.

On the other hand, partial melts, particularly from tholeiitic basalts and to a lesser extent calc-alkaline basaltic amphibolites, yield parent magmas that have lower K_2O and higher (usually greater than 65 wt%) SiO_2 contents, suitable for the differentiation within the tonalite-trondhjemite field. The most suitable source material for the tonalite-trondhjemite magma is, therefore, tholeiitic and calc-alkaline basic rocks. But, the rocks plotting in this field can be subdivided into two geochemically separable types at the 70 wt% SiO_2 level: a high Al-type containing >15 wt% Al_2O_3, and a low-Al type containing <15 wt% Al_2O_3 (Barker et al. 1981). Numerous experimental studies on natural basalt compositions at high pressures (generally >5 kbar) indicate that melts approaching the composition of tonalites and tonalite like melts such as tonalite-trondhjemite-granodiorites (TTG) and adakite have high Al_2O_3 (>15 wt%) and HREE-depleted rare earth element patterns (Rushmer 1991; Beard and Lofgren 1991; Rapp et al. 1991; Şen and Dun 1994; Rapp and Watson 1995; Springer and Seck 1997). However, melts obtained at low pressure (≤ 5 kbar) are distinctly lower in Al_2O_3 than those at higher pressures and also show flat or slightly concave upward REE patterns (Green and Ringwood 1968; Hollaway and Burnham 1972; Helz 1976; Ellis and Thompson 1986; Beard and Lofgren 1989; Springer and Seck 1997). In SiO_2 versus Al_2O_3, CaO and Na_2O Harker variation diagrams (not shown), the felsic rocks of this study are compared with those of liquids experimentally produced at 5 and 10–15 kbar pressures by Springer and Seck (1997). K_2O, Al_2O_3 and CaO contents of the quartz diorites match more with those occurred at 5 kbar. The tonalities and trondhjemites have lower Al_2O_3 (<15 wt%) and CaO (<4 wt%) than 5 kbar melts of Springer and Seck (1997), suggesting that these rocks would be crystallised at much lower pressures (<5 kbar). In addition, they have similar geochemical characteristics to those of low Al-type TTG with their low Al_2O_3 (<15 wt%), low Sr (<200 ppm) contents, lack of any prominent Eu anomaly ($Eu/Eu^* = 0.8–1.1$) and flat HREE patterns (Barker et al. 1981). Besides, flat to slightly LREE-enriched rare earth element patterns (Fig. 7b) suggest the presence of plagioclase and lack of initial garnet extraction as a residue in their genesis. As a result, an origin of tonalitic melts with flat REE patterns at lower crustal depth or mantle must be rejected. Nevertheless, the occurrence of the fact that a tensional and/or transtensional period may lead to form, as a result of rifting, low pressure conditions in the lower crust where basic rocks are found.

Based on these experimental studies and the geochemical characteristics, it can be concluded that the felsic intrusive rocks have resulted from partial melting of basic tholeiitic rocks at lower pressures (< 5 kbar). The presence of former gabbroic rocks of the complex in the area and certain imprints (e.g. gabbro-pegmatites, multiple dike structure and low crystallization pressures of hornblende) of a prevailing extensional period during their emplacement are in agreement with the partial melting of tholeiitic gabbroic or amphibolitic rocks located at the bottom of the intrusive complex. Due to the much higher heat flow in the lower crust during the extensional period, conditions for lower crust melting or former basic rocks could have achieved more easily than during the compressional period. This rationale apparently explains the generation of felsic rocks of the intrusive complex later than mafic rocks. All these corroborate the hypothesis that the tonalites-trondhjemites of the Demirkent intrusive complex have been formed by partial fusion of a basic material of a magmatic arc complex. In addition, REE and major element models suggest that 70–80% fractional melting from a gabbroic source (G694) shows an excellent fit with the primitive varieties of the felsic intrusion (Figs. 17b, 18). The source has the following mineralogy: plagioclase:clinopyroxene:hornblende:magnetite = 54:30:15:1 (Dokuz 2000).

Conditions of the mafic rocks

The temperature and pressure of any magma at the time of intrusion can be estimated on the basis of observed mineral sequences and the chemical composition. In the studied rocks, no olivine and orthopyroxene was observed. Assuming a likely MgO content of 8–10 wt% in the parental basaltic melt, non-crystallization of olivine indicates that the temperature of the parent was lower than 1,000 ± 50°C according to the experiments of Roeder and Emslie (1970). Lack of olivine and orthopyroxene results from the low Fe- and Mg-activity in a residual melt and crystallization of Ca-bearing minerals, such as plagioclase, clinopyroxene and amphibole. Plagioclase is a cumulus phase and included in clinopyroxene indicating crystallization prior to clinopyroxene. This is only possible at pressures below 3 kbar (Green 1982). The needle-shaped plagioclase inclusions, which have An_{71-81} forms at 1,000°C and 2 kbar H_2O pressure (Housh and Lurh 1991). In order to obtain such low temperatures and pressures at the basaltic liquidus, a significant amount of H_2O (5–6 wt%) is necessary (Green 1982; Moore and Carmichael 1988). The agreement of experimental data with observed crystallization sequence and chemical composition of the plagioclase inclusions indicate that the temperature of the parental magma was about 900–1,000°C and the depth of intrusion was approximately 8–10 km. The latter has also been supported by the pressure calculations according to Al-in-horblende (Table 2), and the field and petrographic features, which indicates a period of exhumation prior to the formation of the mafic intrusive rocks. These are the linear shapes of the intrusion on the map view; abundance of hb-rich lithologies; occurrence of microgabbros and micro diorites; volumetrically widespread pegmatitic pods and dikes; absence of olivine and orthopyroxene in crystallization sequence; and widespread transformation of clinopyroxene to hornblende, which all suggest intrusion into a shallow level and/or an extensional condition during the crustal deformation.

Conclusions

The main conclusions drawn from this study are:

1. The low-K mafic and felsic intrusive rocks cross-cutting the Hercynian metamorphic basement in the Eastern Black Sea Region of Turkey are presumably of Early Jurassic age due to a close analogy to the counterparts (184 ± 4.4 Ma) from the Pulur Massif (Bayburt), just southwest of Yusufeli.
2. The geological setting, the rock association, the mineralogy and the chemical composition of the rock types within the intrusive complex all support the hypothesis that the igneous activity in the Yusufeli area occurred above an active subduction zone.
3. The linear shapes of the intrusives on map view, vertical dike structure at the two end points and certain petrographic features including the existence of pegmatites, fine-grained lithologies and low crytallisation temperatures of hornblendes can be interpreted as the result of structural or extensional control on their emplacement during the intra-arc rifting.
4. Variation diagrams and geochemical modelling show that crystal fractionation was the major operating system to produce the evolved lithologies within each body.
5. The major oxide, REE and HFSE compositions of inferred parental rocks to the gabbro-diorite body of the Demirkent intrusive complex can succesfully be generated by 15–20% melting of a lherzolite, probably in the mantle wedge above a subduction zone.
6. Trace element and REE characteristics of the tonalite-trondhjemite body preclude a direct derivation from a mantle wedge. Also, the highly voluminous nature of the felsic body and lack of negative Eu anomalies in the most primitive rocks rules out its derivation from the gabbro-diorite body by fractional crystallization. All the evidence suggests that it could be derived by 70% partial melting of a mafic source, possibly the parent rock of the gabbro-diorite body.

Acknowledgements This paper is improved based on part of the Ph.D. Dissertation of the senior author. We would like to thank our colleagues M. Arslan, M. Akçay and C. Şen for their support and interest during the course of this study, Mehmet Alkan and Rıza Kara, headmen of the Morkaya and Ormandibi villiages, and to the people living in the Yusufeli area for their great hospitality and friendliness during the field studies. We would also like to

thank G. Pe-Piper and J. V. Auwera for constructive reviews that led to numerous improvements in the final manuscript. Financial support for this research was provided by the Research Fund of Karadeniz Technical University.

References

Adamia S, Bayraktutan S, Lordkipanidze MB (1995) Structural correlation and Phanerozoic evolution of the Caucasus-Eastern Pontides. In: Erler A, Ercan T, Bingöl E, Örçen S (eds) Geology of the Black Sea Region, pp 69–75

Akin H (1978) Geologie, Magmatismus und Lagerstaettenbildung im ostpontischen Gebirge-Turkei aus der Sicht der plattentektonik. Geol Rundsch 68:253–283

Akıncı ÖT (1984) The Eastern Pontide volcano-sedimentary belt and associated massive sulphide deposits. In: Dixon JE, Robertson AHF (eds) The geological evolution of the Eastern Mediterranean, vol 17. Geological Society of London Special Publication, London, pp 415–428

Aktimur T, Ateş S, Yurdakul ME, Tekerli ME, Keçer M (1992) Geology of the Niksar-Erbaa and Destek region. Maden Tetkik ve Arama Dergisi 114:25–36

Alp D (1972) Amasya Yöresinin Jeolojisi. Doktora Tezi, İÜ Fen Fakültesi Monografileri Tabii İlimler Kısmı, Sayı, vol 22, 101 pp

Anderson JL, Smith DR (1995) The effect of temperature and oxygen fugacity on Al-in- hornblende barometry. Am Mineral 80:549–559

Barker F (1979) Trondhjemites: definition, environment and hypothesis of origin. In: Barker F (eds) Trondhjemites. Dacites and related rocks. Elsevier, Amsterdam, pp 1–12

Barker F, Arth JG (1976) Generation trondhjemitic-tonalitic liquids and Archean bimodal trondhjemite-basalt suites. Geology 4:596–600

Barker F, Arth JG, Hudson T (1981) Tonalites in crustal evolution. R Soc Lond Philos Transact Ser A 301:293–303

Beard JS, Lofgren GE (1989) Effect of water on the composition of partial melts of greenstone and amphibolite. Science 244:195–197

Beard JS, Lofgren GE (1991) Dehydration melting and water-saturated melting of basaltic and andesitic greenstones and amphibolites at 1.3 and 6.9 kb. J Petrol 32:365–401

Bektaş O, Güven İ (1995) Alaskan-appinic type ultramafic and mafic complexes as the root zone of the Eastern Pontide magmatic arc (NE Turkey). In: Erler A, Ercan T, Bingöl E, Örçen S (eds) Geology of the Black Sea Region, pp 189–196

Bergougnan H (1987) Etudes geologiques dans l'Est Anatolien. PhD Thesis, University Pierre et Marie Curie, 606 pp

Bindeman IL, Davis AM, Drake MJ (1998) Ion microprobe study of plagioclase basalt partition experiments at natural concentration levels of trace elements. Geochim Cosmochim Acta 62:1175–1193

Blundy JD, Holland TJB (1990) Calcic amphibole equilibria and a new amphibole-plagioclase geothermometer. Contrib Mineral Petrol 104:208–224

Brouxel M, Lapierre H, Michard A, Albarede F (1987) The deep layers of a Paleozoic arc: geochemistry of the Copley-Balaklala series, northern California. Earth Planet Sci Lett 85:386–400

Coleman RG (1977) Ophiolites, ancient oceanic lithosphere? Springer, Berlin Heidelberg New York, 201 pp

Coleman RG, Peterman ZE (1975) Oceanic plagiogranite. J Geophys Res 80:1099–1108

Çoğulu E (1975) Gümüşhane ve Rize Granitik Plütonlarının Mukayeseli Petrojeolojik ve Jeokronometrik Etüdü. Doçentlik Tezi, İTÜ, Yayın no: 1034, İstanbul, 112 pp

Davis GA, Monger JWH, Burchviel BC (1978). Mesozoic construction of the Cordilleran 'collage' central British Colombia. In: DG Howell, McDougal KA (eds) Mesozoic Paleogeography of the Western United States, Pasific Section. Society of Economic Paleontologists, Pasific Coast Paleogeography Symposium 2:1–32

Defant MJ, Drummond MS (1993) Mount St Helens Potential example of the partial melting of the subducted lithosphere in a volcanic arc. Geology 21:547–550

Dokuz A (2000) Yusufeli (Artvin-Turkey) yöresinin jeolojisi, jeotektoniği, magmatik-metamorfik kayaçların jeokimyası ve petrojenezi. PhD KTÜ-Trabzon, 311 pp

Ellis DJ, Thompson AB (1986) Subsolidus and partial melting reactions in the quartz-excess $CaO + MgO + Al_2O_3 + SiO_2 + H_2O$ system under water-excess and water-deficient conditions to 10 kbar. Some implications for the origin of peraluminous melts from mafic rocks. J Petrol 27:91–121

Frey FA, Gerlach DC, Hickey RL, Lopez-Escobar L, Munizaga-Villavcencio F (1984) Petrogenesis of the Laguna del Maule volcanic complex, Chile (36° S). Contrib Mineral Petrol 88:133–149

Frey FA, Green EH, Roy SD (1978) Integrated models of basalt petrogenesis: a study of quartz tholeiites to olivine melilites from southeastern Australia, utilizing geochemical and experimental data. J Petrol 19:463–513

Fujimaki H, Tatsumoto M, Aoki K (1984) Partition coefficient of Hf, Zr, and REE between phenocriysts and groundmass. Proceedings of fourteenth lunar and planetary science conference, part 2. J Geophys Res 89(Suppl):B662–B672

Gill JB (1981) Orogenic andesites and plate tectonics. Springer, Berlin Heidelberg New York, 390 pp

Green TH (1982) Anatexis of mafic crust and high pressure crystallization of andesites. In: Thorpe RS (ed) Andesites. Wiley, New York, pp 465–487

Green TH, Ringwood AE (1968) Genesis of calc-alkaline igneous rock suite. Contrib Mineral Petrol 18:105–162

Grove TL, Donnelly-Nolan JM (1986) The evolution of young silicic lavas at Medicine Lake Volcano, California: implications for the origin of compositional gaps in calc-alkaline series lavas. Contrib Mineral Petrol 92:281–302

Hammarstrom JM, Zen E-an (1986) Aluminum in hornblende: an empirical igneous geobarometer. Am Mineral 71:1297–1313

Helz R (1976) Phase relations of basalt in their melting ranges at $P_{H2O} = 5$ kbar. Part 2. Melt compositions. J Petrol 17:139–193

Hirose K (1997) Melting experiment on lherzolite KLB-1 under hydrous conditions and generation of high-magnesian andesitic melts. Geology 25:42–44

Hirose K, Kawamoto T (1995) Hydrous partial melting of lherzolite at 1 GPa: the effect of H_2O on the genesis of basaltic magmas. Earth Planet Sci Lett 133:463–473

Hochstaedter AG, Gill JB, Morris J (1990) Volcanism in the Sumisu Rift, II. Subduction and non-subduction related components. Earth Planet Sci Lett 100:195–209

Hollaway JR, Burnham CW (1972) Melting relations of basalt with equilibrium water pressure less than total pressure. J Petrol 13:1–29

Hollister LS, Grissom GC, Peters EK, Stowell HH, Sisson VB (1987) Confirmation of the empirical correlation of Al in hornblende with pressure of solidification of calc-alkaline plutons. Am Mineral 72:231–239

Housh TB, Lurh JF (1991) Plagioclase-melt equilibria in hydrous system. Am Mineral 76:477–492

Irvine TN (1974) Petrology of the Duke Island ultramafic complex, southern Alaska. Mem Geol Soc Am, vol 138, 240 pp

Irvine TN, Baragar WRA (1971) A guide to chemical classification of the common volcanic rocks. Can J Earth Sci 8:523–548

Irving AJ, Frey FA (1978) Distribution trace elements of between garnet megacrysts and host volcanic liquids of kimberlitic to rhyolitic composition. Geochim Cosmochim Acta 42:771–787

Jahn BM, Vidal P Kroner A (1984) Multi-chronometric ages and origin of Archean tonalitic gneisses in Finnish Lapland: a case for a long crustal residence time. Contrib Mineral Petrol 86:398–408

Johnson MC, Rutherford MJ (1989) Experimental calibration of aluminum-in-hornblende geobarometer with aplication to Long Valley Caldera (California) volcanic rocks. Geology 17:837–841

Kay SM, Kay RW, Citron GP (1982) Tectonic controls on tholeiitic and calc-alkaline magmatism in the Aleutian arc. J Geophys Res 87:4051–4072

Ketin İ (1966) Tectonic units of Anatolia (Asia Minor). Maden Tetkik ve Arama Bulletin 66:23–34

Konak N, Hakyemez HY (1996) Tectonic units of the easternmost part of the Pontides: stratigraphical and structural implications. In: Proceedings of 2nd international symposium on the petroleum geology and hydrocarbon potential of the Black Sea area, pp 32–33

Kushiro I (1990) Partial melting of mantle wedge and evolution of island-arc crust. J Geophys Res 95:15929–15939

Lameyre J, Bowden P (1982) Plutonic rock type series: discrimination of various granitoid series and related rocks. J Volcanol Geotherm Res 14:169–186

Luais B, Hawkesworth CJ (1994) The generation of continental crust: an integrated study of crust forming processes in the Archean Zimbabwe. J Petrol 35:43–93

Martin H (1987) Petrogenesis of Archean trondhjemites, tonalite, and granodiorites from Eastern Finland: major and trace element geochemistry. J Petrol 28:921–953

McCulloch MT, Gamble JA (1991) Geochemical and geodynamical constraints on subduction zone magmatism. Earth Planet Sci Lett 102:258–274

Meijer A (1983) The origin of low-K rhyolites from the Mariana frontal arc. Contrib Mineral Petrol 83:45–51

Michael PJ (1988) The concentration, behavior and storage of H_2O in the suboceanic upper mantle: implication for mantle metasomatism. Geochim Cosmochim Acta 52:555–566

Moore G, Carmichael ISE (1998) The hydrous phase equilibria (to 3 kbar) of an andesite and basaltic andesite from western Mexico: constraints on water content and conditions of phenocryst growth. Contrib Mineral Petrol 130:304–319

Notsu K, Ono K, Soya T (1987) Strontium isotopic relations of bimodal volcanic rocks at Kikai volcano in the Ryikyu arc, Japan. Geology 15:345–348

Okay A (1984) The geology of the Ağvanis metamorphic rocks and neighboring formations. Bull Mineral Res Explor Inst Turkey 99/100:16–36

Okay A (1996) Granulite facies gneisses from the Pulur region, Eastern Pontides. Turk J Earth Sci 5:55–61

Okay A, Şahintürk Ö (1997) Geology of the Eastern Pontides. In: AG Robinson (ed) Regional and petroleum geology of the Black Sea and surrounding region. AAPG Memoir 68:291–311

Ohki J, Shuto K, Kagami H (1994) Middle Miocene bimodal volcanism by asthenospheric upwelling: Sr and Nd isotopic evidence from the back-arc region of the Northwest Japan arc. Geochem J 28:473–487

Pearce JA (1983) Role of the sub-continental lithosphere in magma genesis at active continental margin. In: Hawkesworth CJ, Norry MJ (eds) Continental basalts and mantle xenoliths. Shiva, Chenshire, pp 230–249

Pearce JA, Harris NBW, Tindle AG (1984) Trace element discrimination diagrams for the tectonic interpretation of granitic rocks. J Petrol 25:956–983

Pearce JA, Peate DW (1995) Tectonic implication of the composition of volcanic arc magmas. Ann Rev Earth planet Sci 23:251–285

Peccerillo R, Taylor SR (1976) Geochemistry of Eocene calc-alkaline volcanic rocks from the Kastamonu area, northern Turkey. Contrib Mineral Petrol 58:63–81

Perfit MR, Gust DA, Bence AE, Arculus RJ, Taylor SR (1980) Chemical characteristics of island-arc basalts: implications for mantle sources. Chem Geol 30:227–256

Pouchou JL, Pichoir F (1985) "PAP" $\phi(\rho Z)$ correction procedure for improved quantitative microanalysis. In: Armstrong JT (eds) Microbeam analysis. San Franicisco Press, pp 104–106

Rapp RP, Watson EB (1995) Dehydration melting of metabasalt at 8–32 kbar: implications for continental growth and crust-mantle recycling. J Petrol 36:891–931

Rapp RP, Watson EB, Miller CF (1991) Partial melting of amphibolite/eclogite and origin of Archean trondhjemites and tonalites. Precamb Res 51:1–25

Roeder PL, Emslie RF (1970) Olivin–liquid equilibrium. Contrib Mineral Petrol 29:275–289

Rollinson HR (1993) Using geochemical data. Longman Scientific & Technical, Essex, 352 pp

Rushmer T (1991) Partial melting of two amphibolites: contrasting experimental results under fluid-absent conditions. Contrib Mineral Petrol 107:41–59

Saunders AD, Tarney J, Marsh NG, Wood DA (1980) Ophiolites as an oceanic crust or marginal basin crust: a geochemical approach. In: Panayiotou A (ed) Ophiolites, Proc Int Ophiolite Symp Cyprus 1979. Geol Surv Deep, pp 193–204

Schmidt MW (1992) Amphibole composition in tonalite as a function of pressure: an experimental calibration of the Al-in-hornblende barometer at 650°C, 3.5 kbar. Contrib Mineral Petrol 110:304–310

Snoke AW, Quick JE, Bowman HR (1981) Bear Mountain igneous complex, Klamath Mountains, California: an ultramafic to silicic calc-alkaline suite. J Petrol 22:501–552

Springer W, Seck HA (1997) Partial fusion of basic granulites at 5 to 15 kbar: implications for the origin of TTG magmas. Contrib Mineral Petrol 127:30–45

Stolper EM, Newman S (1994) The role of water in the in the petrogenesis of Mariana trough magmas. Earth Planet Sci Lett 121:293–325

Stormer JC, Nicholls J (1978) XLFRAC: a program for the interactive testing of magmatic differentiation models. Comput Geosci 4:143–159

Streckeisen A (1976) To each plutonic rock its proper name. Earth Sci Rev 12:1–33

Sun SS, McDonough WF (1989) Chemical and isotope systematics of oceanic basalts: implications for mantle compositions and processes. In: Saunders AD, Nory MJ (eds) Magmatism in the ocean basins, vol 42. Geological Society of London Special Publication, London, pp313–345

Şen C, Dunn T (1994) Dehydration melting of a basaltic composition amphibolites at 1.5 and 2.0 GPa: implications for the origin of adakites. Contrib Mineral Petrol 117:394–409

Şengör AMC, Yılmaz Y, Ketin İ (1980) Remnants of Pre-Late Jurassic ocean in northern Turkey fragments of Permian-Triassic Paleo-Tethys. Geol Soc Am Bull 91:599–609

Şengör AMC, Yılmaz Y (1981) Tethyan evolution of Turkey: a plate tectonic approach. Tectonophysics 75:181–241

Tanyolu E (1988) Pulur Masifi doğu kesiminin jeolojisi. Maden Tetkit ve Arama Dergisi 108:1–17

Tatsumi Y (1982) Origin of high-magnesian andesites in the Setouchi volcanic belt, southeast Japan. II. Melting phase relations at high pressures. Earth Planet Sci Lett 60:305–317

Taylor SR, McLennan SM (1985) The continental crust: its composition and evolution. Blackwell, Oxford, 312 pp

Topuz G (2002) Petrology of mafic to ultramafic intrusions from the Pulur Massif, Eastern Pontides, NE Turkey. In: Proceedings of 1st international symposium of the Faculty of Mines (ITU) on earth sciences and engineering, İstanbul, pp 129

Topuz G, Altherr R, Kalt A, Satır M, Werner O, Schwarz WH (2004) Aluminous granulites from the Pulur complex, NE Turkey: a case of partial melting, efficient melt exctraction and crystallization. Lithos 72:183–207

Wilson M (1989) Igneous petrogenesis. Unwin Hyman, London, pp 466

Wood DA, Marsh NG, Tarney J, Joron JL, Fryer P, Treuil M (1981) Geochemistry of igneous rocks recovered from a transect across the Mariana trough, arc, fore-arc, and trench sites 453 through 461. In: Deep Sea Drilling Project Leg 60. Init Rep DSDP 60:611–632

Yılmaz Y (1972) Petrology and structure of the Gümüşhane granite and surrounding rocks, North-Eastern Anatolia, PhD Thesis, University of London, pp 260

Yılmaz Y, Tüysüz O, Yiğitbaş E, Genç ŞC, Şengör AMC (1997) Geology and tectonic evolution of the Pontides. In: Robinson AG (ed) Regional and petroleum geology of the Black Sea and surrounding region. AAPG Memoir 68:183–226